In presenting the dissertation as a partial fulfillment of the requirements for an advanced degree from the Georgia Institute of Technology, I agree that the Library of the Institute shall make it available for inspection and circulation in accordance with its regulations governing materials of this type. I agree that permission to copy from, or to publish from, this dissertation may be granted by the professor under whose direction it was written, or, in his absence, by the Dean of the Graduate Division when such copying or publication is solely for scholarly purposes and does not involve potential financial gain. It is understood that any copying from, or publication of, this dissertation which involves potential financial gain will not be allowed without written permission.

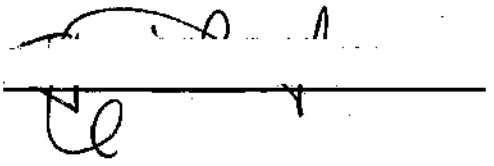

7/25/68

HYDRO-MECHANICAL CONTROL DEVICE FOR STRETCHING CAT MUSCLES

A THESIS

Presented to

The Faculty of the Division of Graduate

Studies and Research

By

Francisco Javier Corral-Aristi

In Partial Fulfillment

of the Requirements for the Degree

Master of Science in Mechanical Engineering

Georgia Institute of Technology

December, 1972

HYDRO-MECHANICAL CONTROL DEVICE

FOR STRETCHING CAT MUSCLES

Approved:

William D. McLeod, Chairman

Stephen L. Dickerson

William D. Letbetter

Prateen V. Desai

Date Approved by Chairman: 12/4/72

ACKNOWLEDGMENTS

The author wishes to express sincere thanks to Dr. William D. McLeod, thesis advisor, for his interest and guidance in this research, to Dr. Stephen L. Dickerson for his assistance during Dr. McLeod's absence and to Dr. Prateen V. Desai.

Special thanks are extended to Dr. William D. Letbetter for his encouragement and active help during the experimental stage of this thesis and also for his patient and helpful work in reviewing the first draft of the thesis.

The author also wishes to thank the "Universidad de Carobobo" in Venezuela whose economic assistance provided him the opportunity to attend graduate school.

Finally, the author wishes to express his deepest gratitude to his wife and son, whose understanding, love and encouragement served as strong incentive during all his graduate work.

TABLE OF CONTENTS

TABLE OF CONTENTS (Continued)

LIST OF TABLES

LIST OF ILLUSTRATIONS

LIST OF ILLUSTRATIONS (Continued)

LIST OF ILLUSTRATIONS (Concluded)

NOMENCLATURE

A	area of piston
Ai	constants (i = 0, 1, . . . 10)
ai	polynomial coefficients (i = 0, 1, 2, . . . 9)
B	a constant, as defined by equation (13)
Bi	constants (i = 1, 2, . . . 10)
C	load damping coefficient
Ce	external leakage coefficient of piston
Ci	internal leakage coefficient of piston
C_t	Ci + Ce/2
C_1	fixed capacitor (lead network)
C_2	variable capacitor (bridged-T)
C_3	fixed capacitor (bridger-T)
E	system's error signal
E_c	bridged-T output voltage
Eo	lead network output voltage
F	force transmitted to and from load
$G_d(s)$	system's open loop transfer function (displacement)
$G_f(s)$	system's open loop transfer function (force)
$H_d(s)$	system's closed loop transfer function (displacement)
$H_f(s)$	system's closed loop transfer function (force)
I	valve input current
K	a constant as defined by equation (17)

NOMENCLATURE (Continued)

Ka	electronic amplifier gain
K_f	a constant as defined by equation (14)
K_L	a constant as defined by equation (13)
K_t	feedback potentiometer constant
K_{tf}	force transducer gain
Kv	valve flow gain
K_1	spring constant of load
L	a constant as defined by equation (18)
M	$M_L + M_P$
M_L	equivalent mass of muscle
M_P	mass of piston, rod and transducers
P_1	forward pressure
P_2	return pressure
P_L	$(P_1 + P_2)/2$
Q_1	flow into forward chamber
Q_2	flow into return chamber
Q_L	valve flow $((Q_1 + Q_2)/2)$
R	variable resistor (bridged-T)
R_1	variable resistor (lead network)
R_2	variable resistor (lead network)
s	Laplace operator
t	time
T_1	time constant of lead circuit for break-up frequency

NOMENCLATURE (Concluded)

T_2	time constant of lead circuit for breakdown frequency
V	step input magnitude
Vi	system's input
Vo	system's output
Vr	slope of the ramp input
V_1	volume of the forward chamber
V_2	volume of the return chamber
Vo_1	V_1 initial
Vo_2	V_2 initial
V_t	total volume under compression
x	mechanical output position
βe	effective builk modulus
ω_f	load natural frequency
ω_h	hydraulic natural frequency
ω_p	natural frequency at poles (bridged-T)
ω_v	apparent natural frequency of the valve
ω_z	natural frequency at zeros (bridger-T)
ξ_f	load damping ratio
ξ_h	hydraulic damping ratio
ξ_p	damping ratio of poles (bridged-T)
ξ_v	apparent damping ratio of the valve
ξ_z	damping ratio of zeros (bridged-T)

SUMMARY

The present study deals with the design, construction, and testing of an electro-hydraulic control system capable of providing the control of force or displacement of living cat muscles in neurophysiological studies.

The system is designed to allow control of either output force or position. Mathematical analysis of the system is carried out to show that, in the case when displacement is the controlled variable, the response of the system is not satisfactory. This deductions incorporated to design a compensating network that theoretically shows a more satisfying range of operation. Likewise when force is the controlled variable, the theoretical analysis shows that the closed-loop is unstable. The use of another compensating network, which happens to be the same as part of the network used for the position system, produces a satisfactory response and the system is placed within specifications.

The compensated design is used to fabricate and test the system for frequency and time domain performance. Comparison of the theoretical approach with the results obtained experimentally shows a fairly good agreement for the case in which displacement is the controlled variable. With force as the controlled variable some differences are found between theory and experiments. The main reason for this disagreement is thought to be the simplified model used for representing the muscle dynamics. However, there is not available

any better model that could be used easily in a practical way. Nevertheless, all the specifications imposed on the system, both for control and measurement of force and displacement are met. Therefore, the development of a device which can be usefully employed in neurophysiological studies of muscle mechanics and muscle sensory receptors has been successfully accomplished.

CHAPTER I

INTRODUCTION

History and Description of the Problem

It has been known for over one hundred years that muscle contains a variety of nervous structures. Early histological studies begun in the 1860's finally led to the realization in the 1890's that there were two main sensory organs which had definite form and probable relevance to the detection of muscle activity. These are the Golgi tendon organ (named after the man who first described it -- Camillo Golgi) and the muscle spindle (so called for its fusiform shape). Further histological studies, both by light microscopy and by electron microscopy, have revealed that the muscle spindle is an extremely conplicated structure and is one of the most intricately organized sensory organs in the body (second in complexity only to the eye). We now know that the muscle spindle contains within it two separate types of sensory nerve fibers, two separate types of muscle fibers, and two separate types of motor nerve fibers supplying the contained muscle fibers. Therefore, the muscle spindle is a structure whose sensory output can be controlled via a motor input from the central nervous system.

J. F. Fulton and J. Pi-Suñer (1928)[1] had pointed out that, on theoretical grounds, a difference in behavior was to be expected between the tendon organ and the muscle spindle in view of the fact

that the tendon organs are situated in series with the working muscle fibers of a muscle, while the muscle spindle is arranged in parallel with the same fibers. They concluded that both endings should respond to muscle stretch, but that the spindle endings should be unloaded during a muscle contraction, when the whole muscle shortens, while the tendon organ endings should still be experiencing stretch. When B. H. C. Matthews (1933)[2] provided the first comprehensive description of the behavior of single afferent fibers from muscle receptors, this was exactly the sort of interpretation he was able to give to the discharge patterns he saw. Since then, and most notably since the early 1950's, a large number of investigations have been carried out on muscle receptors to determine what parameters they are capable of measuring. It has been concluded that the discharge patterns from the tendon organ receptors may code tension, while one of the muscle spindle receptors codes length and the other codes both length and rate of change of length. Since the tendon organs provide negative feedback upon the motor output centers to the muscles from which they arise, and at least one of the spindle endings provides positive feedback upon these same motor centers, it appears that reflex muscle control (at least at the spinal cord level) may take place through some process which can be described in terms of control systems theory, as R. E. Poppele and C. A. Terzuolo [3] did in 1968.

In order to study motor control processes quantitatively, it became important to have some device which allowed the carefully controlled excitation of muscle sensory organs and the input-output relations between the sensory receptors, the spinal motor control

centers, and muscle. The many mechanical devices designed in the past for this type of study have generally been open-loop systems and only in some more recent models has feedback control been employed to form a servomechanism. Furthermore, most of the recent models have been large and bulky, since most of them employed some sort of electromagnetic vibrator as the displacement device.

In view of the recent "engineering approaches" to muscle and its neurologic control (e.g., R.E. Poppele and R.J. Bowman [4], 1970; N.P. Rosenthal, et al. [5], 1970; W. J. Roberts, et al. [6], 1971) and because of the necessity for clearly classifying both motor and sensory elements in neuromuscular studies, there is a need for a muscle pulling machine which is of reasonable size, of adequate strength, and is easily controlled.

The specifications which need to be met by the displacement and force measuring devices are clear from the literature on the use of these devices. However, the constraints that need to be met by the feedback control device are not so clear. Therefore, initial specifications for these parameters were estimated and a system was designed to satisfy them. These specifications are listed below:

a- Measurement

1- Force

.0 to 10 Kgms (±.5 grams)

2- Displacement

.0 to 25 mm (±.1 mm)

b- Control

1- Force

.0 to 10 Kgms (±.2 percent)

2- Displacement

.0 to 25 mm (±.2 percent)

3- Transient Response

Rise time < .5 sec

4- Frequency Response

i- Gain attenuation < 70 percent at 60 cps

ii- Phase lag < 180^{o} at 60 cps

Review of Literature

Several mechanical systems have been developed to produce stretches in muscles during the past 15 years. D. R. Wilkie [7], M. M. Civan and R. J. Podolsky [8], H. L. McCrovey, et al. [9], and G. Lennerstrand and U. Thoden [10], to name a few, have reported the use of weights, stops, ergometers, levers, and so on to produce ramp stretching at supposedly constant velocities.

D. Stuart, et al. [11], and P. B. C. Matthews and R. B. Stein [12] have also used these same kind of systems to produce sinusoidal stretching.

A hydraulic pump and cylinder was used by E. Alnaes, et al [13] to produce velocities of stretch of about 18 mm/sec. The system was open-loop and controlled by a series of electromagnetic valves.

In 1959 P. B. C. Matthews [14] used a semi-closed loop system to stretch cat soleus muscles at rates that he reported to be between

1 mm/sec and about 6 mm/sec. The arrangement that he used is shown in Figure 1. Basically it consists of an electrical motor coupled to a screw thread through an electromagnetic clutch and a pair of gears. The displacement was measured by a current generator and was fed back to a difference amplifier with compared this signal with the command voltage used as the input. The error signal was then fed to the electrical motor. The system that he used seems to be full of inertial forces, friction, and backlash problems. Furthermore, no measurement of the real position of the muscle was made and,therefore, the system from this point of view is open-loop.

N. P. Rosenthal, et al. [5] used an open loop system to stretch triceps surae muscles of cats in 1970. They applied sinusoidal and step stretches using a d.c. motor coupled to a cam-lever system. This permitted them to change the amplitude of the sine wave. The frequency was varied changing the velocity of the d.c. motor. The step stretches were produced by two solenoids wired to pull in opposite directions. The step amplitude of the solenoid was adjusted manually and its displacement was recorded by a transducer. Force and displacement were measured by two transducers connected in series and located between the muscle and the device. Obviously the accuracy of this device is limited as no signal is fed back, resulting in an open-loop system. Its versatility is also very poor as sinusoids and steps were the only two possible inputs to the muscle.

N. F. Clinch and V. A. Tennant [15] have developed a loudspeaker servo system for use in studying muscle mechanics which was reported

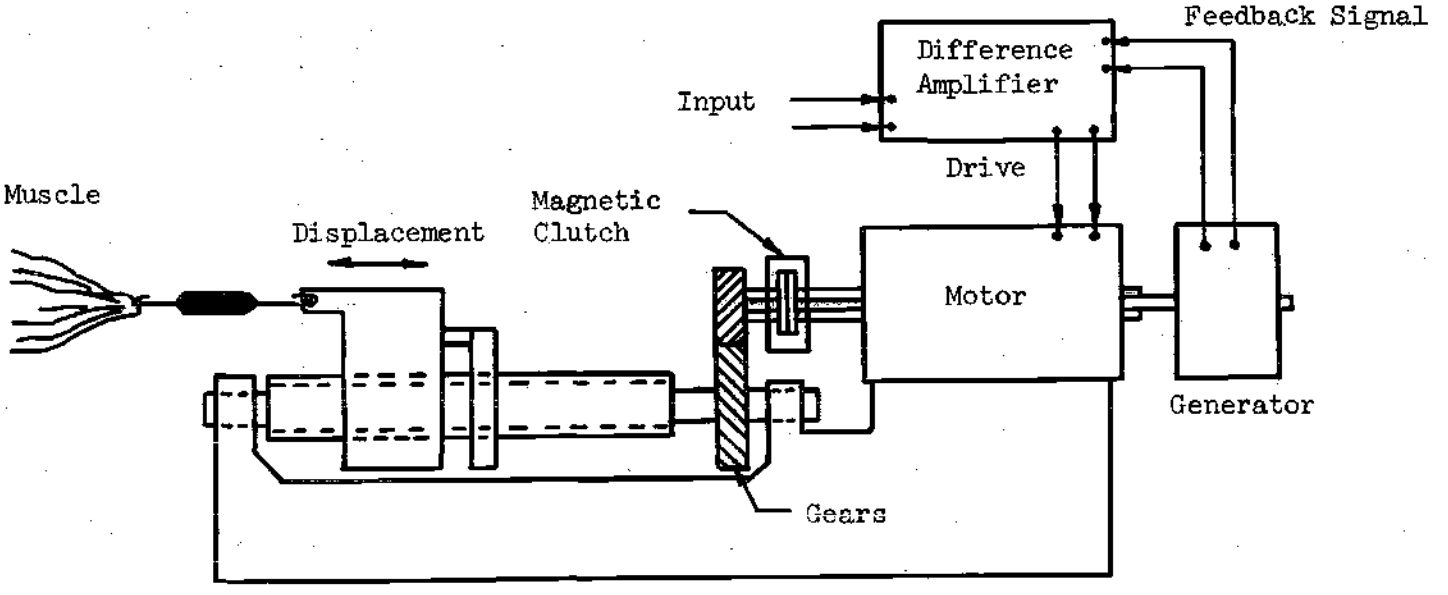

Figure 1. Servo-Motor Driven Mechanical Stimulator.

recently (May 1972). The scheme of this system is shown in Figure 2. It consists of a modified loudspeaker mounted rigidly on a brass framework on which is also mounted a light source-lens-photocell system that acts as a displacement transducer. The signal produced by the photocell is fed into an electronic amplifier and compensating network. This arrangement permits the comparison of the input signal or reference signal to the actual position of the muscle and the subsequent application of a correcting signal to the loudspeaker coil for repositioning the muscle. With the inclusion of the compensating network,consisting of two lead-lags and a lag-lead, they have obtained a bandwidth of 240 cps. The main limitation of this device is its minimum travel, which is on the order of 4 mm. Its range of force is also very small. As a consequence of this, the system cannot be applied to large muscle systems such as those of the cat. K. E. Machin and J. W. Pringle [16], M. C. Brown, et al.[17], P. B. C. Matthews [18], and other have reported the use of devices very similar to the loudspeaker system described in the preceeding paragraph. However, the band widths in these were considerably narrower than that reported by Clinch.

There are bigger versions of the loudspeaker commercially available, but as the power source. Several problems are associated with them; the large size, open loop characteristic, and low resonant frequencies are their main limitations. The size is increased because the ratio of power to force is of the order of 10 amperes/kilogram. The resonant frequency is about 100 cps for small forces and as low as 10 cps for the more powerful ones.

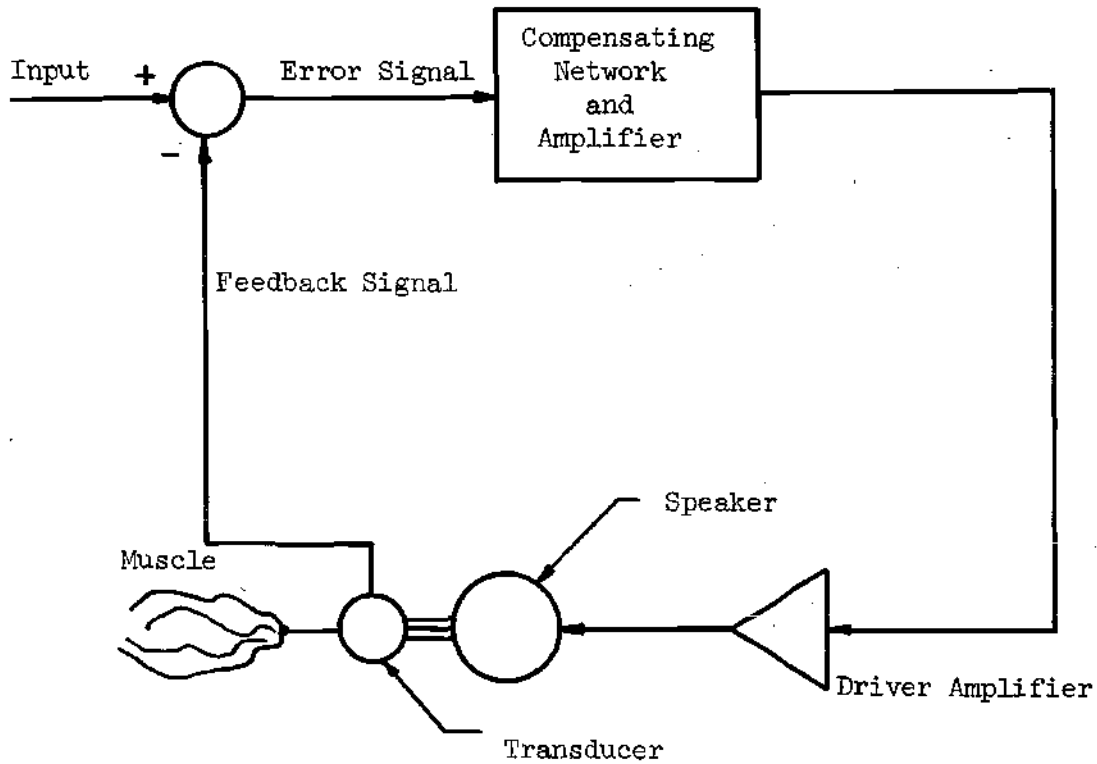

Figure 2. Loudspeaker Servo-System.

Proposed Solution and Scope of the Research

As a possible solution to the problem the design, fabrication and testing of an electrohydraulic control system was proposed. The design was carried out to meet the specifications previously stated. This kind of system provides a more versatile device for stretching muscles at different rates, amplitudes and input functions.

The system, as developed and built, permits the application of controlled forces or displacements (one at a time) to the muscle, while simultaneously measuring both force and displacement continuously. Its size is small compared with the big version of the commercially available loudspeaker-type system.

CHAPTER II

THEORETICAL ANALYSIS

System Description

The proposed solution to the problem of concern is a constant-supply-pressure electrohydraulic control system. A schematic diagram of it is shown in Figure 3. It can be seen that a differential d-c electronic amplifier is used to compare the input and feedback signals and to amplify the resultant error. The output of this amplifier is fed to a four-way, two stage electrohydraulic servovalve which controls the flow of oil to a double acting hydraulic cylinder. The cylinder rod is directly attached to the load (cat muscle). The displacement and force applied are detected by a rectilinear feedback potentiometer and a Wheatstone bridge force transducer. The type of feedback is selected by a solid state switch module which is operated by a logic signal from a digital computer, which has been previously programmed. The command signal (or reference value) is also provided by the computer through a digital/analog converter. A more detailed description of each component is given in Appendix II.

Mathematical Model

In the next paragraphs the linear mathematical model of each component is evaluated and finally all those transfer characteristics are combined to obtain the open and closed loop transfer function of the system for displacement and force feedback. Figure 4 shows the

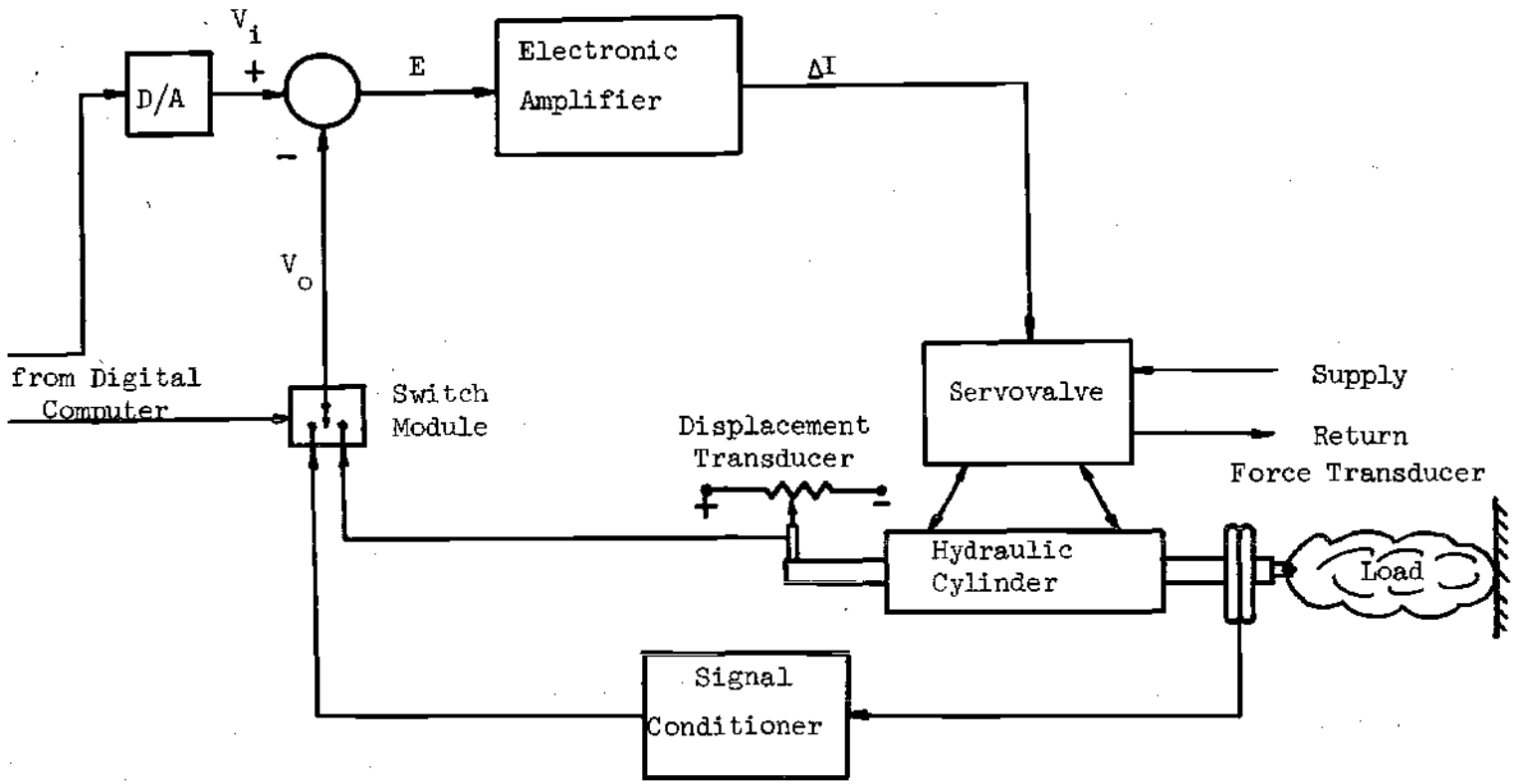

Figure 3. Schematic Diagram of the System.

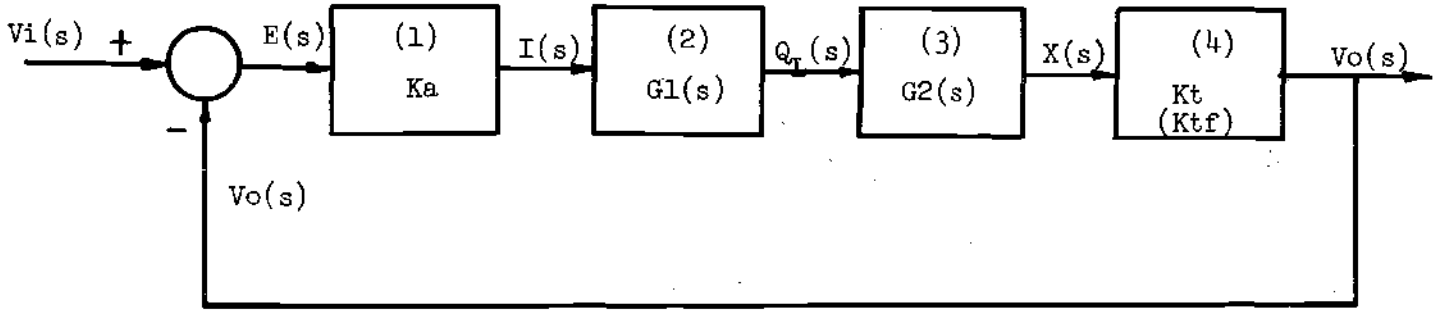

(1) Amplifier

(2) Servovalve

(3) Cylinder and Load

(4) Transducer

Figure 4. Block Diagram of the System.

overall block diagram corresponding to the scheme of Figure 3, on which basis the study was done.

Amplifier Transfer Function

The amplifier transfer characteristic is given by

$$\frac{I(s)}{E(s)} = Ka \qquad (1)$$

where

E = Error signal, Volts

I = Output current, mA

Ka = Amplifier gain, mA/Volts

S = Laplace operator

Servovalve Transfer Function

A two-stage, four-way, mechanical feedback, electrohydraulic servovalve could be represented by a third or higher order nonlinear transfer function, but in servoanalysis the usefulness of linear transfer functions for approximating servovalve response is well established [19], [20], [21]. According to the specifications, the system of concern is intended to work at frequencies of 60 cps or lower. Therefore, a linear second-order empirical approximation is sufficient for the analysis of the complete system. Hence the servovalve transfer function is assumed to be

$$\frac{Q_L(s)}{I(s)} = Kv \frac{\omega_v^2}{s^2 + 2\xi_v\omega_v s + \omega_v^2} \qquad (2)$$

where

Kv = valve flow gain, $in^3/sec/mA$

ω_v = apparent valve natural frequency, rad/sec

ξ_v = apparent valve damping ratio

s = Laplace's operator

Q_L = valve output flow, in^3/sec

I = valve input current, mA

The values of ω_v and ξ_v are furnished by the manufacturer, according to experimental results.

Cylinder and Load Transfer Function

The following assumptions are made in evaluating the cylinder transfer function according to the pattern given by H. E. Merrit [22]:

(1) Linear analysis is applicable

(2) The piston is centered

(3) The friction forces can be neglected

(4) The velocities in the chambers are small so that minor losses are negligible

(5) Line phenomena are absent

(6) Temperature and density of the working fluid are constant

(7) Linearized about at rest conditions

Applying the continuity equation to each of the piston chambers yields (see Figure 5):

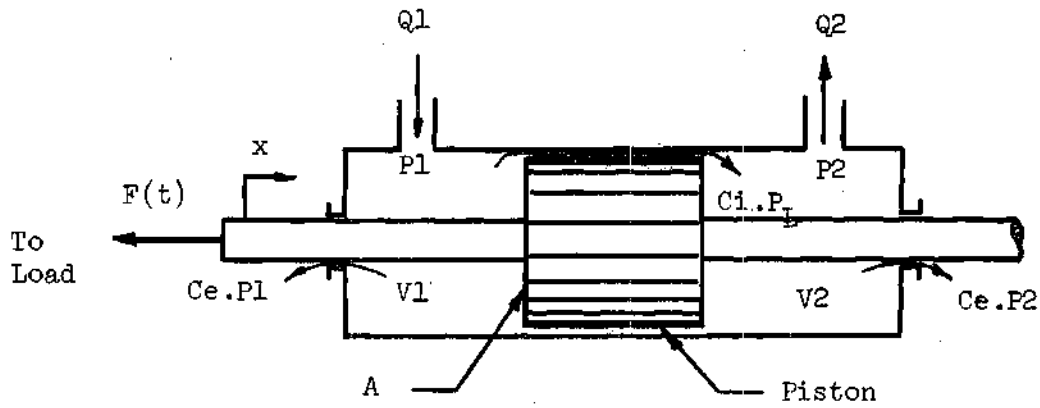

x = Rod end displacement, in.

A = Area of piston, in^2.

Q1 = Flow into forward chamber, in^3/sec.

Q2 = Flow into return chamber, in^3/sec.

P1 = Forward pressure, psi

P2 = Return pressure, psi.

P_L = P1-P2, psi

V1 = Volume of forward chamber (Includes valve and connecting line), in^3.

V2 = Volume of return chamber (Includes valve and connecting line), in^3.

VO1 = V1 initial, in^3

VO2 = V2 initial, in^3

βe = Effective bulk modulus (includes oil entrapped and mechanical compliance), psi

Ci = Internal leakage coefficient of piston, $in^3/sec/psi$.

Ce = External leakage coefficient of piston, $in^3/sec/psi$.

t = Time, sec.

F = Force due to the load, lb.

Figure 5. Cylinder Cross Section and Symbols.

$$Q_1 - Ci(P_1-P_2)-CeP_1 = \frac{dV_1}{dt} + \frac{V_1}{\beta e}\frac{dP_1}{dt} \tag{3}$$

$$-Q_2 + Ci(P_1-P_2)-CeP_2 = \frac{dV_2}{dt} + \frac{V_2}{\beta e}\frac{dP_2}{dt} \tag{4}$$

V_1 and V_2 are related to V_{01} and V_{02} by

$$V_1 = V_{01} + Ax(t) \tag{5}$$

$$V_2 = V_{02} - Ax(t) \tag{6}$$

If piston centered

$$V_{01} = V_{02} = V_0 \tag{7}$$

Thus

$$V_1 + V_2 = 2V_0 = V_t \tag{8}$$

where

V_t = total volume of fluid under compression.

The combination of equations (3) through (8) and its Laplace transformation yields

$$Q_L(s) = Asx(s) + C_tP_L + \frac{V_t}{4\beta e} s P_L \tag{9}$$

where

$$Q_L = \frac{Q_1 + Q_2}{2} = \text{Load flow, } in^3/sec$$

$$C_t = Ci + Ce/2 = \text{Total leakage coefficient, } in^3/sec/psi$$

Applying Newton's second law to the forces acting on the piston and Laplace transforming

$$AP_L = M_p s^2 X(s) + F(s) \qquad (10)$$

where

M_p = Mass of piston, rod and transducers, $(lb\text{-}sec^2)/in$

To complete the cylinder and load transfer function it is necessary to assume a mechanical configuration of a muscle. A. Crowe [23] and J. W. Pringle [24] have developed theoretical muscle models in terms of springs and viscous dampers, but not verified experimentally. Due to the wide variation in the behavior of these components for different biological situations and the imposibility of obtaining values for the parameters, a more simple representation is assumed for the present work.

The model chosen is formed by a mass connected to a spring and viscous damper arranged in parallel, as shown in Figure 6. The reasons for using this model are that in that way, it is possible to get an experimental spring constant for the muscle to evaluate an equivalent mass and, assuming that the model is overdamped, to determine the damping coefficient. The evaluation of these parameters

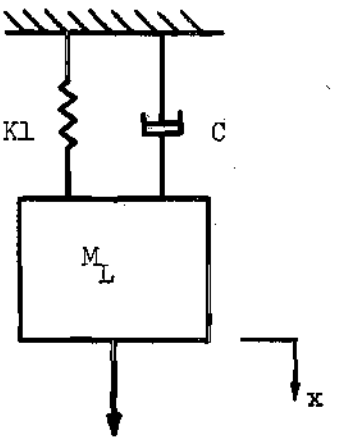

M_L = Equivalent mass of muscle, lb-sec^2/in.

Kl = Linear spring constant, lb/in.

C = Damping ratio, lb-sec/in.

F = Force applied by the cylinder, lb.

x = Displacement, in.

Figure 6. Muscle Model and Symbols.

is shown in Appendix I. If a more complicated model were used the representation would be probably more accurate mathematically, but without any method to determine the parameters. With reference to Figure 6, applying Newton's second law and Laplace transforming, the resulting equation of motion is

$$F(s) = M_L s^2 X(s) + Cs X(s) + K_1 X(s) \tag{11}$$

The combination of equations (9), (10) and (11) yields

$$\frac{X(s)}{Q_L(s)} = \frac{\dfrac{4\beta e A}{4\beta e A^2 + 4C_t C\beta e + V_t K_1}}{s\{[\dfrac{V_t M}{4\beta e A^2+4C_t C\beta e+V_t K_1}]s^2+[\dfrac{4C_t M \beta e + V_t C}{4\beta A^2+4C_t C\beta e+V_t K_1}]s+1\}+\dfrac{4\beta e K_1 C_t}{4\beta e A^2+4C_t C\beta e+V_t K_1}} \tag{12}$$

or in the reduced form

$$\frac{X(s)}{Q_L(s)} = K_L \frac{\omega_h^2}{s(s^2 + 2\xi_h \omega_h s + \omega_h^2)+ B} \tag{13}$$

where:

$$\omega_h = \left(\frac{4\beta e A^2 + 4C_t C\beta e + V_t K_1}{V_t M}\right)^{\frac{1}{2}}$$

= Hydraulic natural frequency, rad/sec.

$$\xi_h = 2C_t\beta e \left(\frac{M}{V_t[4\beta eA^2 + 4C_tC\beta e + V_tK_1]}\right)^{\frac{1}{2}} +$$

$$+ \frac{C}{2}\left(\frac{V_t}{M[4\beta eA^2 + 4C_tC\beta e + V_tK_1]}\right)^{\frac{1}{2}}$$

= Hydraulic damping ratio

$$K_L = \frac{4\beta eA}{4\beta eA^2 + 4C_tC\beta e + V_tK_1}$$

$$B = \frac{K_LK_1C_t\omega_h^2}{A^2}$$

$$M = M_p + M_L$$

= Total mass, lb-sec^2/in.

Equation (13) gives the cylinder and load transfer function, for the condition of displacement feedback control.

For the case of force beedback control, the algebraic manipulation of equations (11) and (13) yields

$$\frac{F(s)}{Q_L(s)} = \frac{K_f\,\omega_h^2\,(s^2 + 2\xi_f\,\omega_f s + \omega_f^2)}{s(s^2 + 2\xi_h\,\omega_h s + \omega_h^2) + B} \qquad (14)$$

where

$$K_f = K_LM_L$$

$\omega_f = (K_l/M_L)^{\frac{1}{2}}$ = Load natural frequency, rad/sec

$\xi_f = C/2\ (1/M_L K_l)^{\frac{1}{2}}$ = Load damping ratio.

Transducer Transfer Function

The relation between output voltage and displacement is

$$\frac{Vo(s)}{X(s)} = K_t \tag{15}$$

where

Vo = System output, Volts

K_t = Feedback potentiometer constant, Volts/in.

The relation between output voltage and force is

$$\frac{Vo(s)}{F(s)} = K_{tf} \tag{16}$$

where

K_{tf} = Force transducer gain, Volts/lb.

Open Loop Transfer Function

The block diagram of Figure 4 can be reduced to a single block in the forward path, as shown in Figure 7a. G(s) represents the open loop transfer function which is obtained by the combination of equations (1), (2), (13), and (15), for the displacement feecback case (defined as $G_d(s)$). For the case of force feedback, the open loop transfer function is defined by $G_f(s)$ and is obtained by combination of equations (1), (2), (14) and (16). Thus,

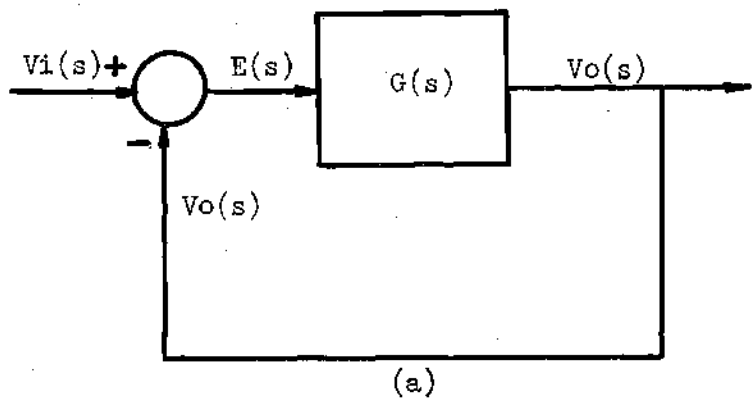

(a)

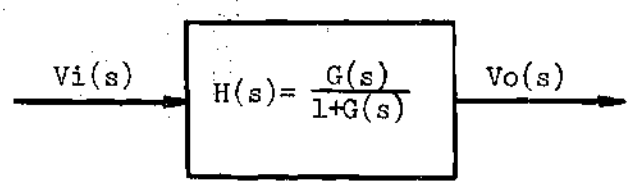

(b)

Figure 7. (a) Reduced Block Diagram
(b) System Reduced to a Single Block.

$$G_d(s) = \frac{K}{[s^2+2\xi_v\omega_v s + \omega_v^2]\,[s(s^2 + 2\xi_h\omega_h s + \omega_h^2) + B]} \tag{17}$$

where

$$K = KaK_vK_tK_L\omega_v^2\omega_h^2$$

and

$$G_f(s) = \frac{L\,[s^2+2\xi_f\omega_f s+\omega_f^2]}{[s^2+ 2\xi_v\omega_v s + \omega_v^2]\,[s(s^2 + 2\xi_h\omega_h s + \omega_h^2) + B]} \tag{18}$$

where

$$L = KaK_vK_fK_{tf}\omega_v^2\omega_h^2$$

Closed Loop Transfer Function

The closed loop transfer function for a unity feedback system is given by

$$H(s) = \frac{G(s)}{1+G(s)} \tag{19}$$

For the displacement case, equation (19) becomes

$$H_d(s) = \frac{K}{[s^2+2\xi_v\omega_v s+\omega_v^2]\;\;[s(s^2+2\xi_h\omega_h s + \omega_h^2) + B]+ K} \tag{20}$$

For the force case, equation (19) becomes

$$H_f(s) = \frac{L[s^2+2\xi_f\omega_f s+\omega_f^2]}{[s^2+2\xi_v\omega_v s+\omega_v^2][s(s^2+2\xi_h\omega_h s+\omega_h^2)+B]+L[s+2\xi_f\omega_f+\omega_f^2]} \qquad (21)$$

System Response Analysis

Displacement Feedback

In order to determine the stability and frequency response of the system, both Bode diagrams (the open and closed loop) were obtained for different conditions of load and selected parameters. The computer program which was developed and used to carry out tnis study is presented in Appendix III.

Only two parameters were varied, the effective bulk modulus (βe) and the total leakage coefficient in the cylinder (C_t). They were chosen because of the difficulty of estimating them and because of their pronounced influence on the resonant frequency and damping ratio. Furthermore, the remaining parameters are known, within a close margin of approximation, once the components are selected as shown in Appendix II.

For industrial design purposes βe is assumed to be equal to 10^5 psi and C_t to be 4 percent of the maximum flow per psi. As the present work is more involved than an industrial system, a sensitivity analysis was performed in which βe was allowed to vary from 10^5 psi to 1.5×10^5 psi and C_t from .00001 to .00005 $in^3/sec/psi$. These range of values are what should be expected for this kind of system.

The numerical analysis of the expresions for ω_h and ξ_h shows that the maximum range for the localization and the magnitude of the

resonant peak is fixed by the combination of the maximum and minimum values of these parameters (i.e., $\beta e = 10^5$ psi and $C_t = .00005$ in^3/sec/psi or $\beta e = 1.5 \times 10^5$ psi and $C_t = .00001$ in^3/sec/psi). Other parameters affected by βe and C_t are the constants K_L and B.

If the system is considered without load, B goes to zero and K_L increases due to the absence of the muscle spring constant and damping coefficient. ω_h and ξ_h vary for the same reason.

The values of these constants for the combinations considered are shown in Table 1. The rest of the parameters used are given on Appendix II, where the components of the system are specified.

Replacing s by $j\omega$ in equations (17) and (20) and letting ω vary, the Bode plots of Figures 8 to 11 were obtained. Figures 8 and 9 show the effect of varying the load for $\beta e = 10^5$ psi and $C_t = .00005$ in^3/sec/psi. Figures 10 and 11 show the same effect but for $\beta e = 1.5 \times 10^5$ psi and $C_t = .00001$ in^3/sec/psi.

From all these plots it can be concluded that the system with displacement feecback is stable for all the conditions considered. However, there is a resonant peak that occurs between 1,250 and 2,400 rad/sec whose magnitude increases as the resonant frequency (ω_h) increases. It can be seen also that the gain ratio is very poor for frequencies higher than 30 rad/sec. On the other hand, the response under these conditions will be quite oscillatory and will exhibit high overshoots.

A consequence of these observations is the necessity to add some kind of compensation to the system in order to improve its response.

Table 1. Variation of Parameters with βe, C_t and Load for Displacement Feedback.

	βe = 100,000 psi C_t = .00005 $in^3/sec/psi$		βe = 150,000 psi C_t = .00001 $in^3/sec/psi$	
System Parameters	Loaded	Unloaded	Loaded	Unloaded
K_L	4.9971	5.00	4.9993	5.00
B	18,302.4	.00	5,490.7	.00
ω_h	1,255.11	1,907.01	1,536.85	2,335.60
ξ_h	.0291	.0154	.0104	.0038

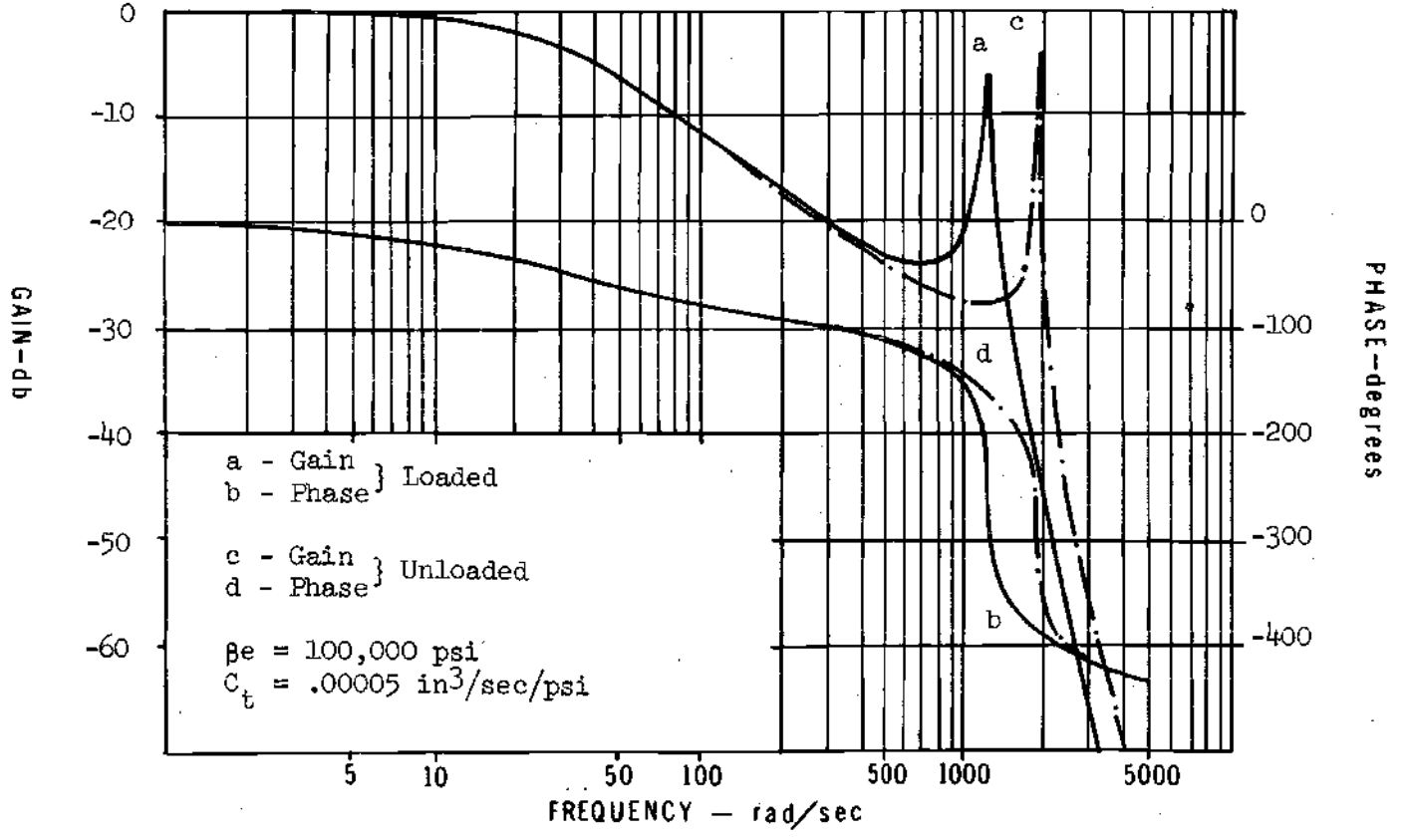

Figure 8. Closed-Loop Frequency Responce Showing the Effect of Varying the Load. Displacement Output.

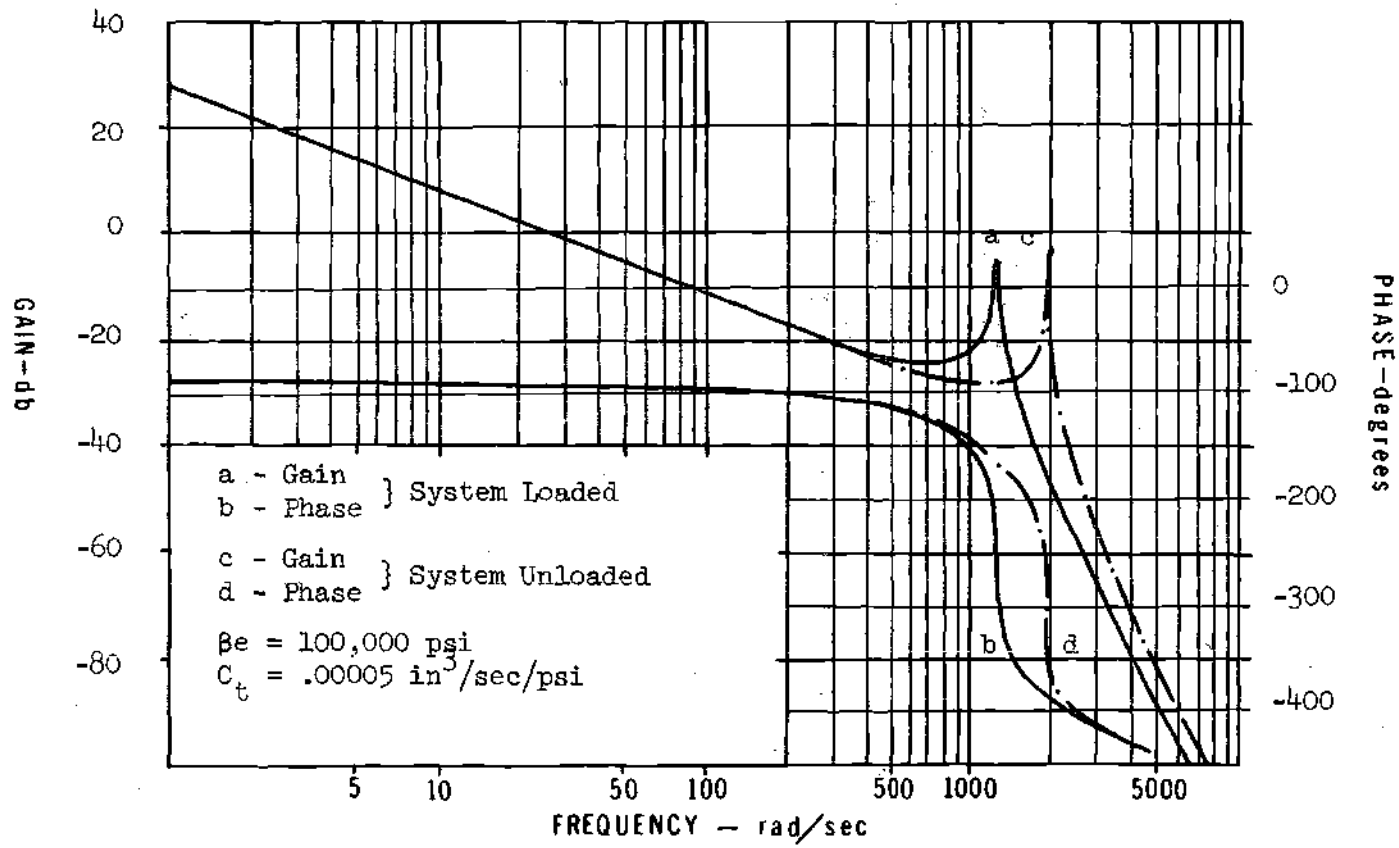

Figure 9. Open-Loop Frequency Response Showing the Effect of Varying the Load. Displacement Output.

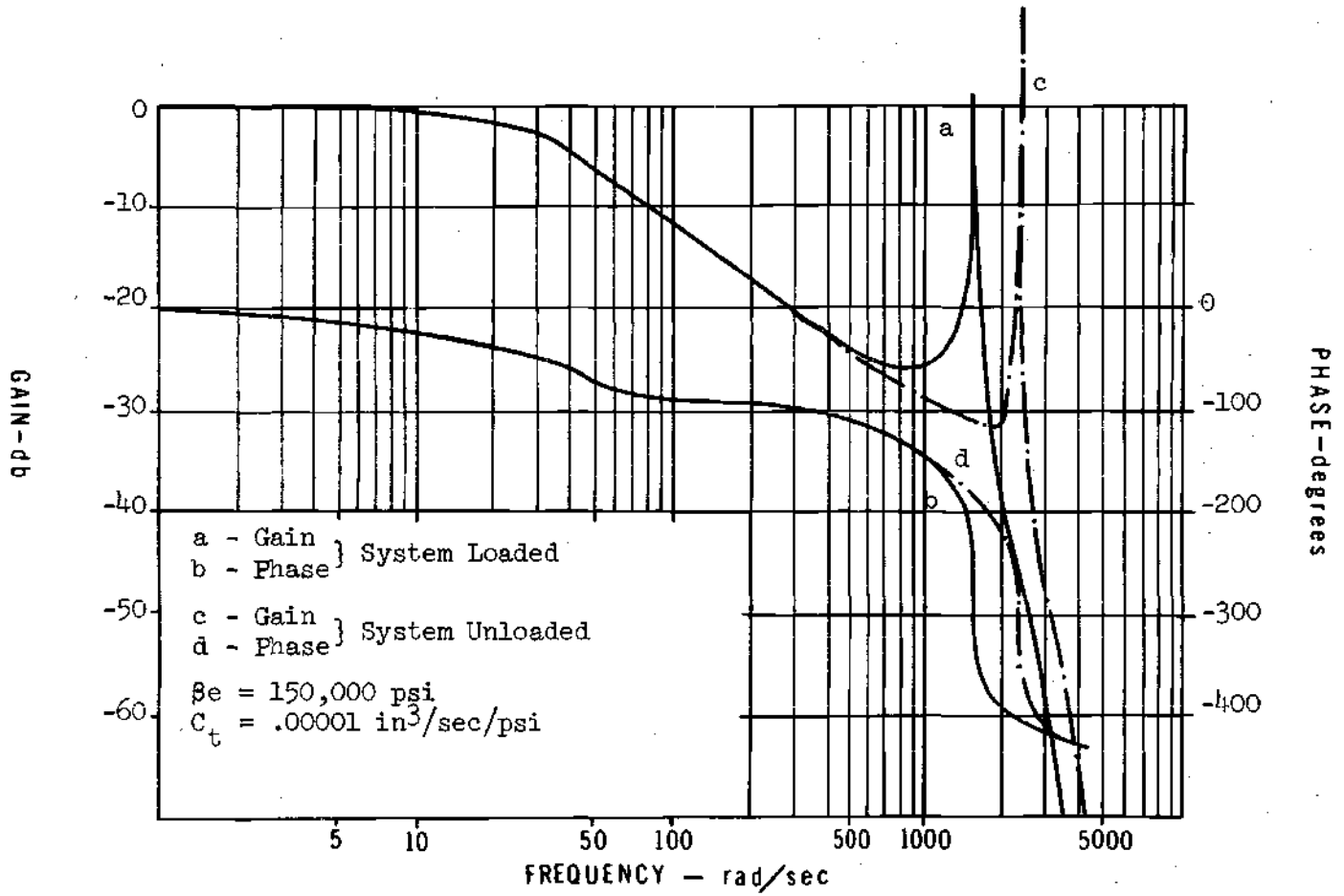

Figure 10. Closed-Loop Frequency Response Showing the Effect of Varying the Load. Displacement Output.

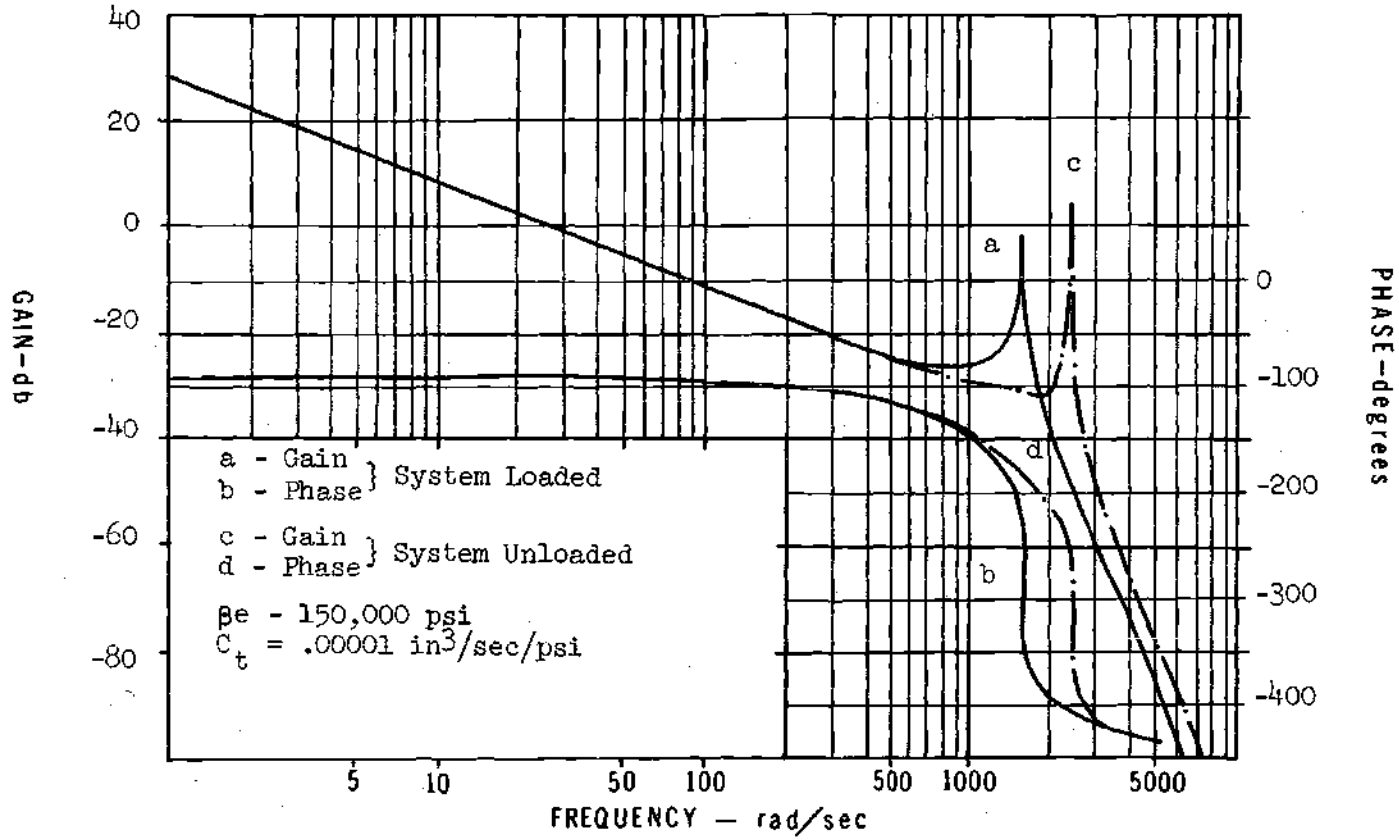

Figure 11. Open-Loop Frequency Response Showing the Effect of Varying the Load. Displacement Output.

Force Feedback

As in the case of displacement feedback, a theoretical study of the system response was performed but this time only the parameters βe and C_t were varied, as the no-load condition for this case is meaningless. ω_h and ξ_h are also affected by βe and C_t and vary in the same fashion as before. The constants K_f and B also change, but the former is defined as $K_L M_L$ which makes the change in it practically unappreciable (as it can be seen from Table 2).

Using a computer program similar to the one used for the case in which the controlled variable is displacement, and replacing s by $j\omega$ in equation (18), the open loop Bode plot was obtained. It is shown in Figure 12.

From there, it can be seen clearly that for a phase angle of -180° the gain ratio is greater than 50 db for any condition of βe and C_t. Thus the system is very unstable. Obviously, the time response of the system would be unacceptable under these conditions. Therefore, it is not necessary to perform a closed-loop Bode plot for the system. As a consequence of this it is imperative to use compensation to send the system into an operative region.

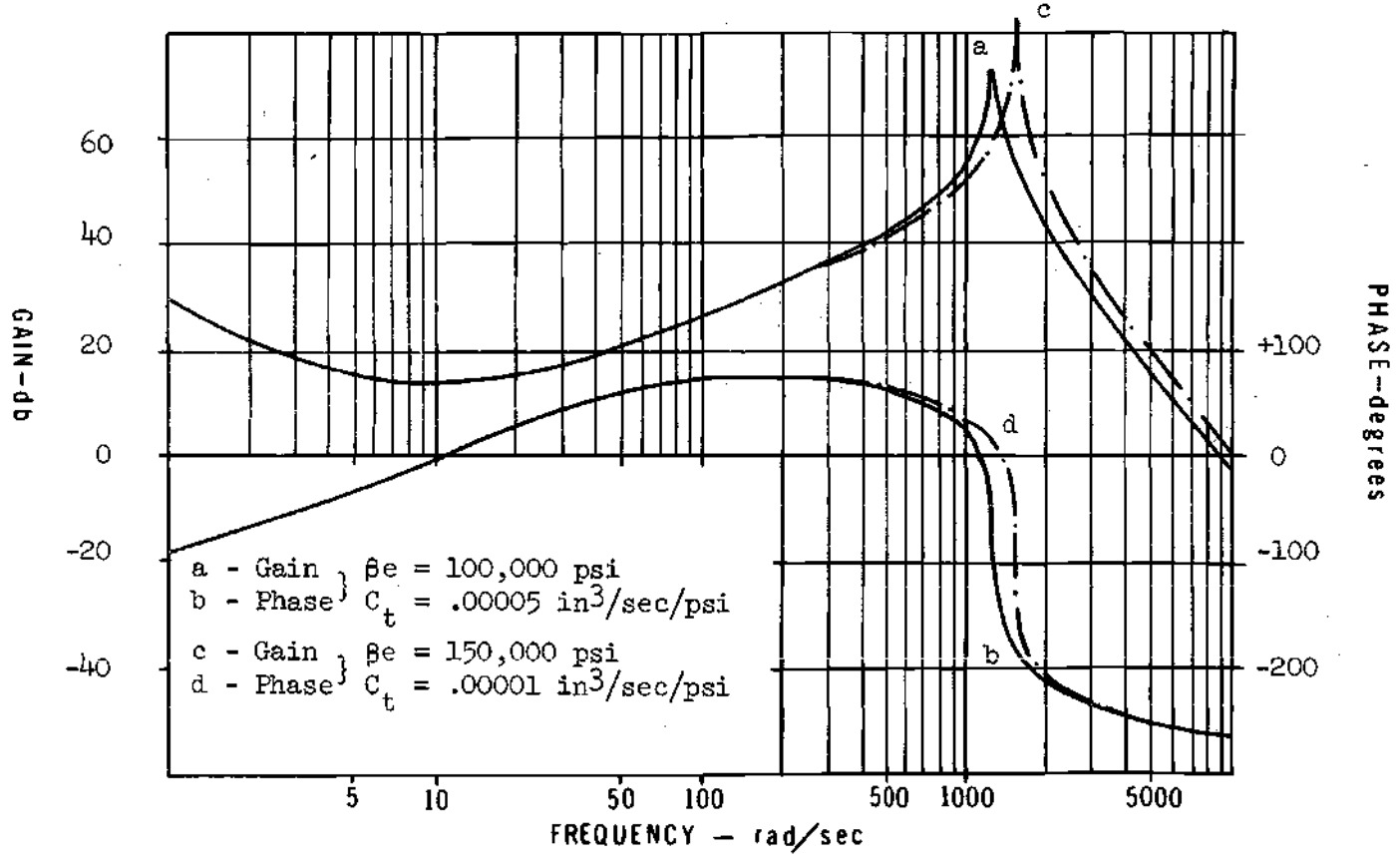

Figure 12. Open-Loop Frequency Response Showing the Effect of Varying βe and C_t. Force Output.

Table 2. Variation of Parameters* with βe and C_t for Force Feedback.

Parameters	βe = 100,000 psi C_t = .00005 $in^3/sec/psi$	βe = 150,000 psi C_t = .00001 $in^3/sec/psi$
K_f	.08470	.08473
B	18,302.40	5,490.72
ω_h	1,255.11	1,536.85
ξ_h	.0291	.0104

*See Appendix II for the other pertinent parameters not affected by βe and C_t.

CHAPTER III

IMPROVING THE RESPONSE OF THE SYSTEM

Need for Compensation

The frequency response analysis performed in Chapter II showed that, in the case where displacement was the controlled variable the system exhibited a high resonant peak and poor gain ratio. Furthermore, if force was the controlled variable the closed loop system was unstable. It is evident then that in either of the cases considered, the system behavior is not very desirable and compensation should be introduced. The present chapter is devoted to the design of compensating networks for both cases, force and displacement, and is followed by a theoretical prediction of the compensated system response.

Displacement Feedback Compensator

For this case, two passive networks are introduced in the forward path of the system. The first one is used to attenuate the resonant peak and the second to improve the gain ratio.

Resonant Peak Attenuation

From Table 1 and Figures 8 through 11 it is obvious that the resonant peak is due to a pair of complex conugated poles near the imaginary axis and is produced by the hydraulic natural frequency (ω_h) and the low damping ratio (ξ_h) associated with it.

P. Chandaket and A. B. Rosenstein [25] give a compensating method that is based on the nearly exact cancellation of the two complex conjugated poles (which cause the oscillations) with two zeros obtained from the simple R-C passive network, shown in Figure 13a. With reference to Figure 13a, and assuming zero input impedance and infinite load impedance, the so called bridged-T network transfer function is found to be

$$\frac{E_c(s)}{E(s)} = \frac{s^2 + 2\xi_z \omega_z s + \omega_z^2}{s^2 + 2\xi_p \omega_p s + \omega_p^2} \qquad (22)$$

where

E_c = Output voltage, Volts

E = Input voltage (system's error), Volts

$$\omega_z = \omega_p = \frac{1}{R(C_2C_3)^{\frac{1}{2}}} \text{ , rad/sec}$$

$$\xi_z = (C_2/C_3)^{\frac{1}{2}}$$

$$\xi_p = \frac{1 + 2\xi_z^2}{2\xi_z}$$

So, if ω_h and ξ_h are to be cancelled

$$\omega_p = \omega_z = \omega_h$$

$$\xi_z = \xi_h$$

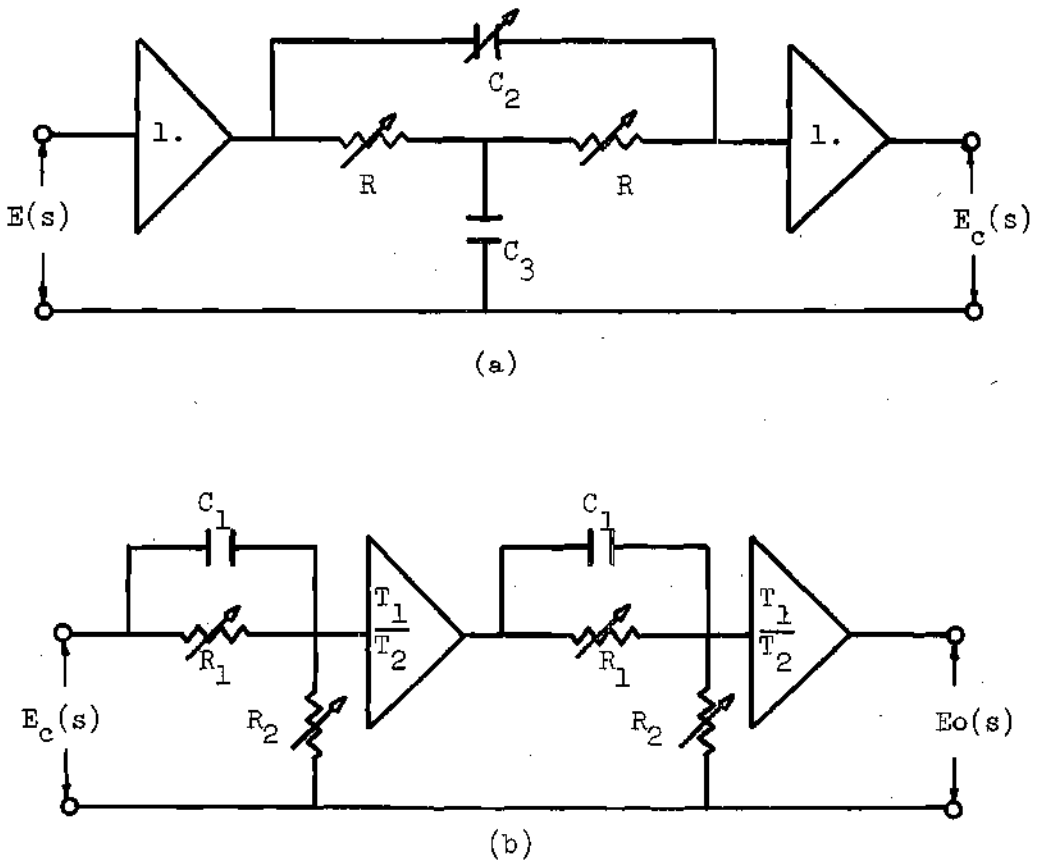

Figure 13. Compensating Networks
(a) Bridged-T
(b) Two Lead Networks in Series

$$\xi_p = \frac{1 + 2\xi_h^2}{2\xi_h}$$

and the bridged-T transfer function to be used becomes

$$\frac{E_c(s)}{E(s)} = \frac{s^2 + 2\xi_h \omega_h s + \omega_h^2}{s^2 + 2\xi_p \omega_h s + \omega_h^2} \tag{23}$$

From the definition of ω_z, ω_p, ξ_z, and ξ_p expressions for C_2, C_3 and R are found as follows:

$$C_2 = C_3 \xi_h^2, \text{ farads} \tag{24}$$

$$R = \frac{1}{\omega_h (C_2 C_3)^{\frac{1}{2}}}, \text{ ohms} \tag{25}$$

Substituting in the values of ω_h and ξ_h (C_3 is set arbitrarily), the resistances and capacitors can be selected as shown in Appendix IV.

With the inclusion of this network, the closed loop frequency response of the system is obtained typically as shown by Figure 14. It should be noted that, the resonant peak has been eliminated but the gain ratio still remains very poor for frequencies higher than 30 rad/sec.

Gain Ratio Improvement

From the last Bode plot (Figure 14), the gain curve has a negative slope of 40 db/decade. So, if two first-order lead passive

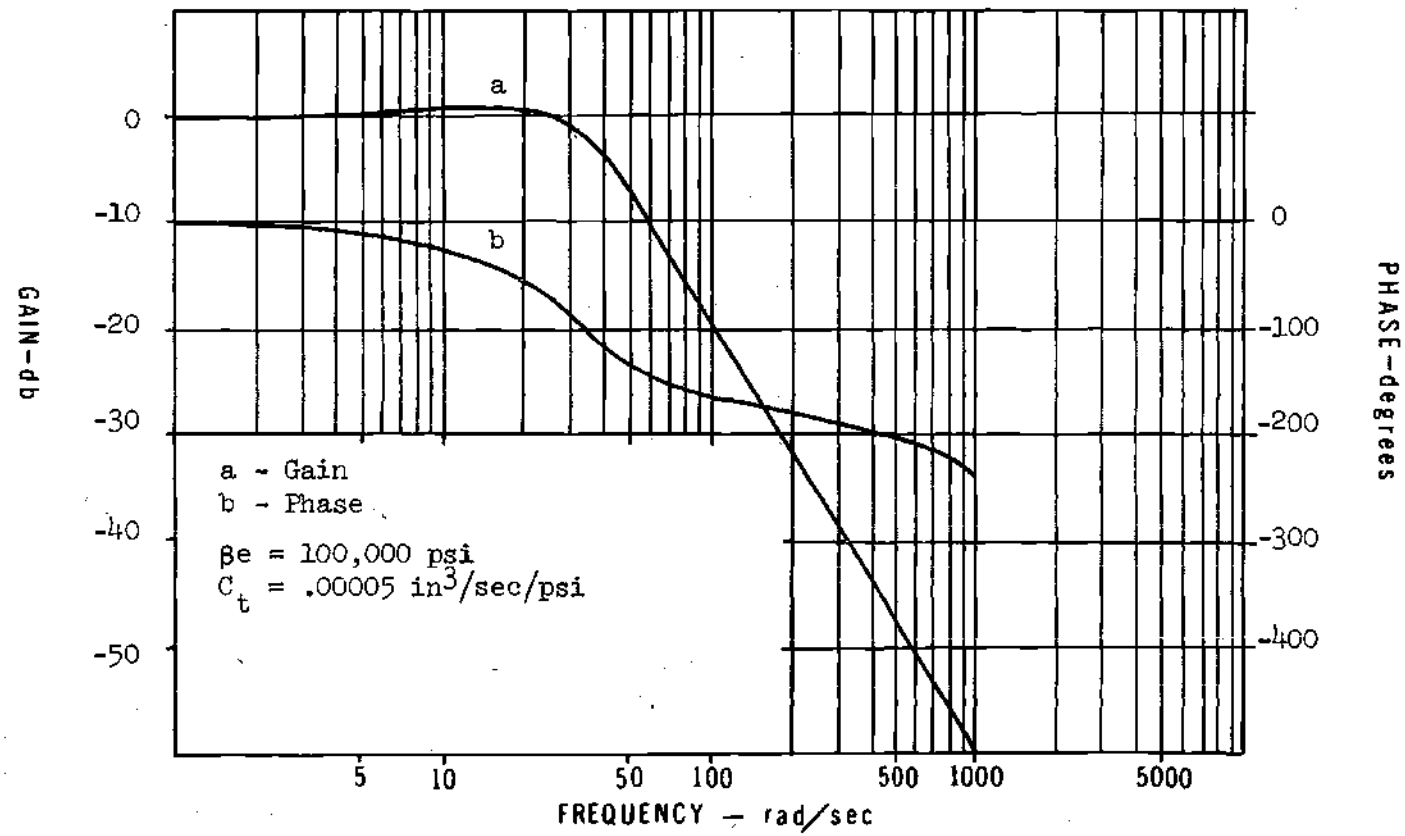

Figure 14. Closed-Loop Frequency Response for the Loaded System After the Inclusion of the Bridged-T Network. Displacement Output.

networks are connected in parallel with the bridged-T in the forward path, the gain ratio is improved considerably. In fact, it is brought into the range of interest for the system of concern. The transfer function of the two lead circuits in parallel (shown in Figure 13b) with the assumption of zero input impedance and infinite load impedance is

$$\frac{Eo(s)}{E_c(s)} = \frac{(T_2/T_1)^2(1 + T_1 s)^2}{(1 + T_2 s)^2} \tag{26}$$

where

Ec = Input voltage (Output of bridged-T), Volts

Eo = Output voltage, Volts

$T_1 = R_1 C_1$, sec.

$T_2 = R_2/(R_1+R_2) \cdot T_1$, sec.

$T_1 > T_2$

Two operational amplifiers were included to counteract the d-c attenuation produced by $(T_2/T_1)^2$ and to approximate the condition of infinite load impedance and zero input impedance. From the definition of T_1 and T_2, the expressions for R_1 and R_2 are found to be

$$R_1 = \frac{T_1}{C_1}, \text{ ohms} \tag{27}$$

$$R_2 = \frac{T_2 R_1}{T_1 - T_2}, \text{ ohms} \tag{28}$$

Therefore, by choosing the proper values of T_1 and T_2 (C_1 set arbitrarily) the resistances to be used can be evaluated. This was done in Appendix IV.

System Response - Displacement Feedback

Frequency Response

Once the compensating network is included the open loop transfer function of the displacement feedback system becomes

$$G_d(s) = \frac{K(1+T_1 s)^2(s^2+2\xi_h\omega_h s+\omega_h^2)}{[s^2+2\xi_v\omega_v s+\omega_v^2][s(s^2+2\xi_h\omega_h s+\omega_h^2)+B][1+T_2 s]^2[s^2+2\xi_p\omega_h s+\omega_h^2]} \quad (29)$$

and the closed loop one

$$H_d(s) = \frac{G_d(s)}{1+G_d(s)} \quad (30)$$

From equations (29) and (30) the open and closed loop Bode plots (shown in Figures 15 to 17) were obtained for different values of T_1, T_2, βe, C_t and load.

The range selected for T_1 to vary is from .033 sec to .1 sec. This allows a break frequency varying between 10 rad/sec and 30 rad/sec. From Figure 14, it is seen that this is the range of interest on which the gain ratio must be improved. By the same kind of reasoning T_2 was varied from .033 sec to .01 sec with the corresponding break frequency varying between 100 rad/sec and 300 rad/sec. The definitive values of T_1 and T_2 are selected in the experimental work by making a

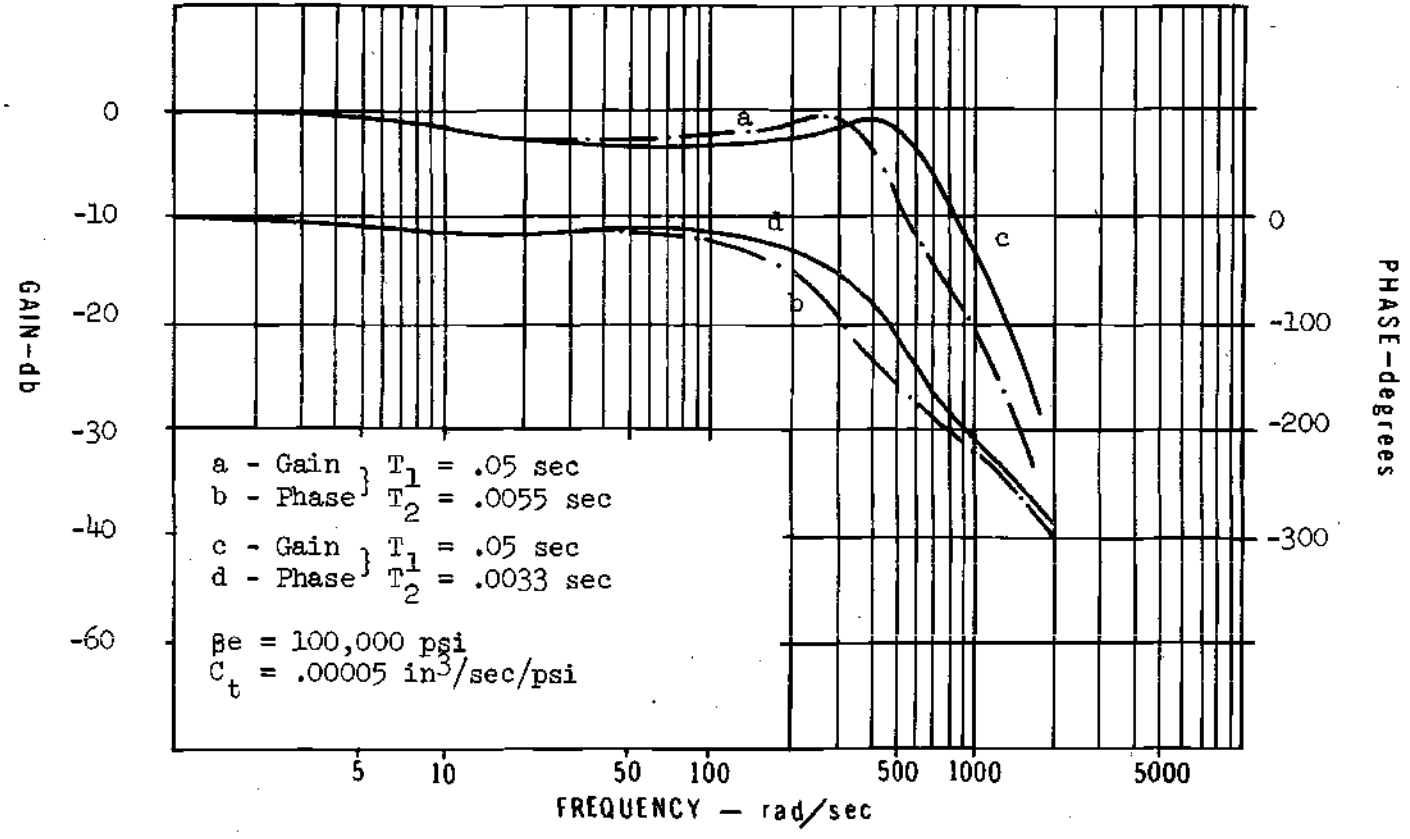

Figure 15. Closed-Loop Frequency Response Showing the Effect of Varying T_1 and T_2. Displacement Output Without Load.

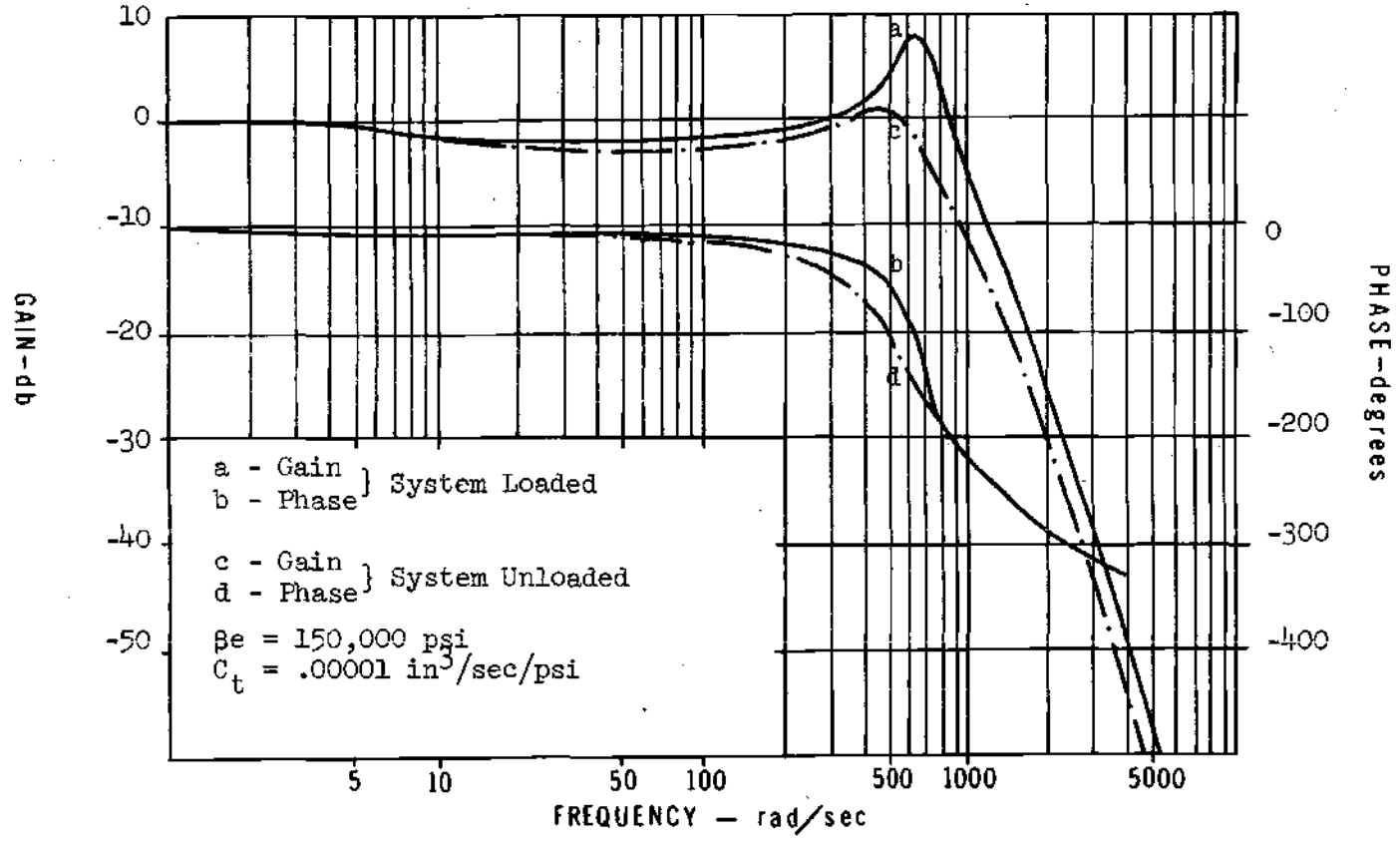

Figure 16. Closed-Loop Frequency Response Showing the Effect of Varying the Load for T_1 = .1 sec and T_2 = .0033 sec. Displacement Output.

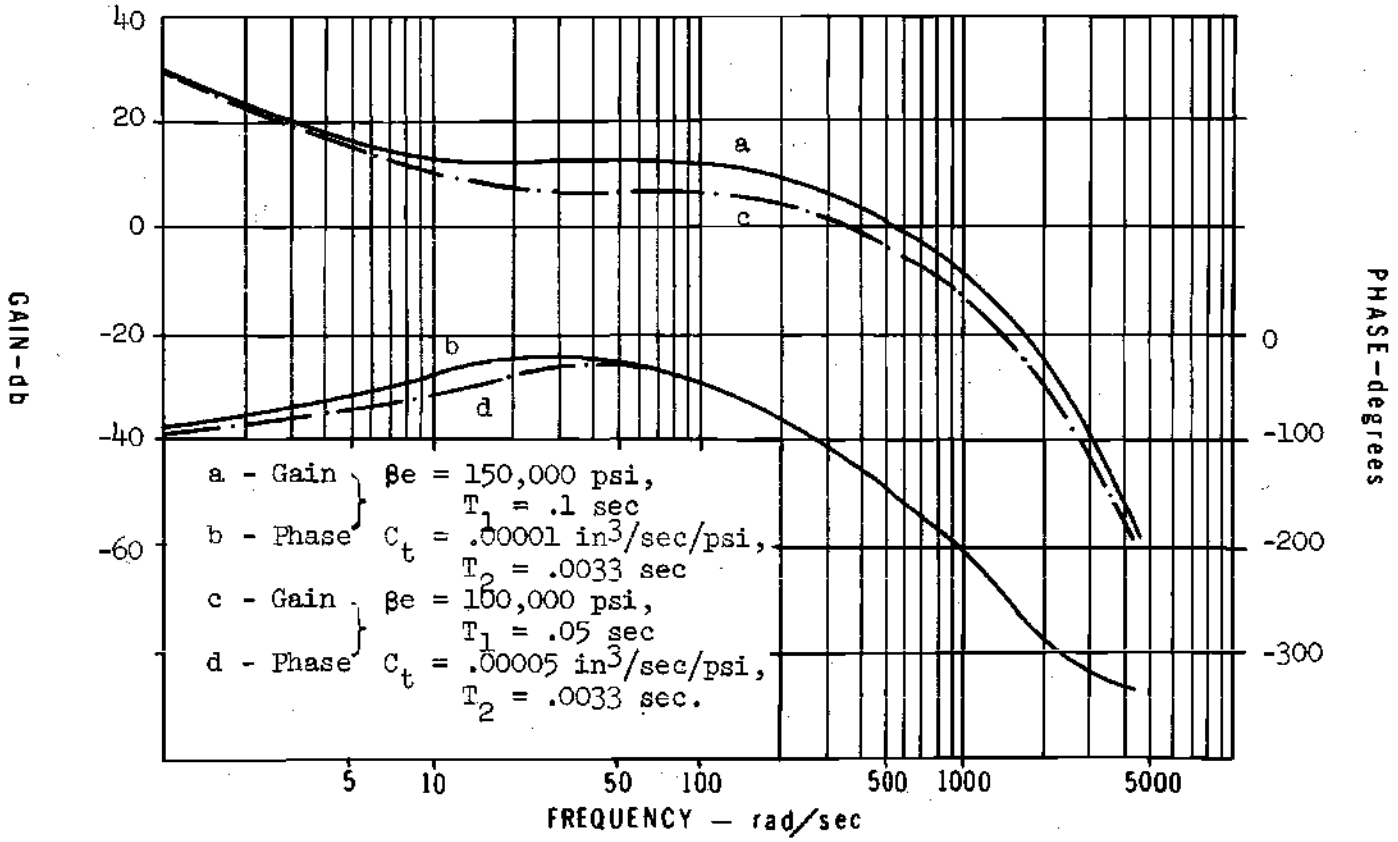

Figure 17. Open-Loop Frequency Response for Two Typical Situations. Displacement Output with Load and Compensation.

compromise between response and the stability.

Figure 15 shows the influence of varying T_1 and T_2. Figure 16 shows the effect of the load. The combination of both Figures 15 and 16 shows the influence of βe and C_t. Figure 17 gives the open loop plot for two typical cases. From these graphs it can be seen that the resonant peak has been attenuated and the gain ratio has acceptable values for frequencies up to 500-700 rad/sec.

Transient Response

Equation (30) can be expressed in the form

$$H_d(s) = \frac{K(1+T_1 s)^2(s^2+2\xi_h\omega_h s+\omega_h^2)}{a_9 s^9+a_8 s^8+a_7 s^7+a_6 s^6+a_5 s^5+a_4 s^4+a_3 s^3+a_2 s^2+a_1 s+a_0} \qquad (31)$$

where the a_i's are the coefficients that result from the multiplication of the denominator factors of equation (30).

For a step input

$$\frac{Vo(t)}{Vi(t)} = \frac{Vo(t)}{V} = H_d(t) \qquad (32)$$

where

Vo(t) = System's input, Volts

Vi(t) = System's output, Volts

V = Magnitude of the step, Volts

or, in the Laplace's domain,

$$\frac{Vo(s)}{V} = \frac{H_d(s)}{s} \tag{33}$$

If this last equation is broken into partial fractions

$$\frac{H_d(s)}{s} = \frac{B_1}{s} + \frac{B_2}{s-r_1} + \frac{B_3}{s-r_2} + \frac{B_4}{s-r_4} + \ldots + \frac{B_{10}}{s-r_9} \tag{34}$$

where

ri = roots of characteristic equation $(G_d(s)+1=0)$

Bi = constants

Now, taking the inverse Laplace transforms of equation (34), the response of the system to a step input in dimensionless form is

$$\frac{Vo(t)}{V} = B_1 + B_2 e^{r_1 t} + B_e e^{r_2 t} + \ldots + B_{10} e^{r_9 t} \tag{35}$$

If a ramp input is considered

$$\frac{Vo(t)}{Vi(t)} = \frac{Vo(t)}{V_r t} = H_d(t) \tag{36}$$

where

V_r is the slope of the input ramp (V/sec).

In the Laplace transform domain

$$\frac{Vo(s)}{V_r} = \frac{H_d(s)}{s^2} \tag{37}$$

and by the same procedure than before the dimensionless response of the system is

$$\frac{Vo(t)}{V_r} = A_0 + A_1 t + A_2 e^{r_1 t} + A_3 e^{r_2 t} + \ldots + A_{10} e^{r_9 t} \qquad (38)$$

where the Ai's are the constants that result from breaking equation (37) into partial fractions.

All these algebraic manipulations were performed with the aid of a digital computer (see Appendix III). Figures 18 and 19 show the predicted transient response of the system for different situations that may occur in the experimental phase of the present work.

From both Figures it is readily seen that for a step input, the load contributes to a more oscillatory and slower response. As T_1 increases, both the time required to reach the steady state and the amplitude of the overshoot get larger. For a ramp input the differences in the response are not very noticeable, except for times less than 100 milliseconds.

Steady State Error

The steady state error, as defined by H. L. Harrison and J. G. Bollinger [26] is

$$e_{ss}(t) = \lim_{s \to 0} s\, E(s)$$

where

$e_{ss}(t)$ = Steady state error $(t \to \infty)$

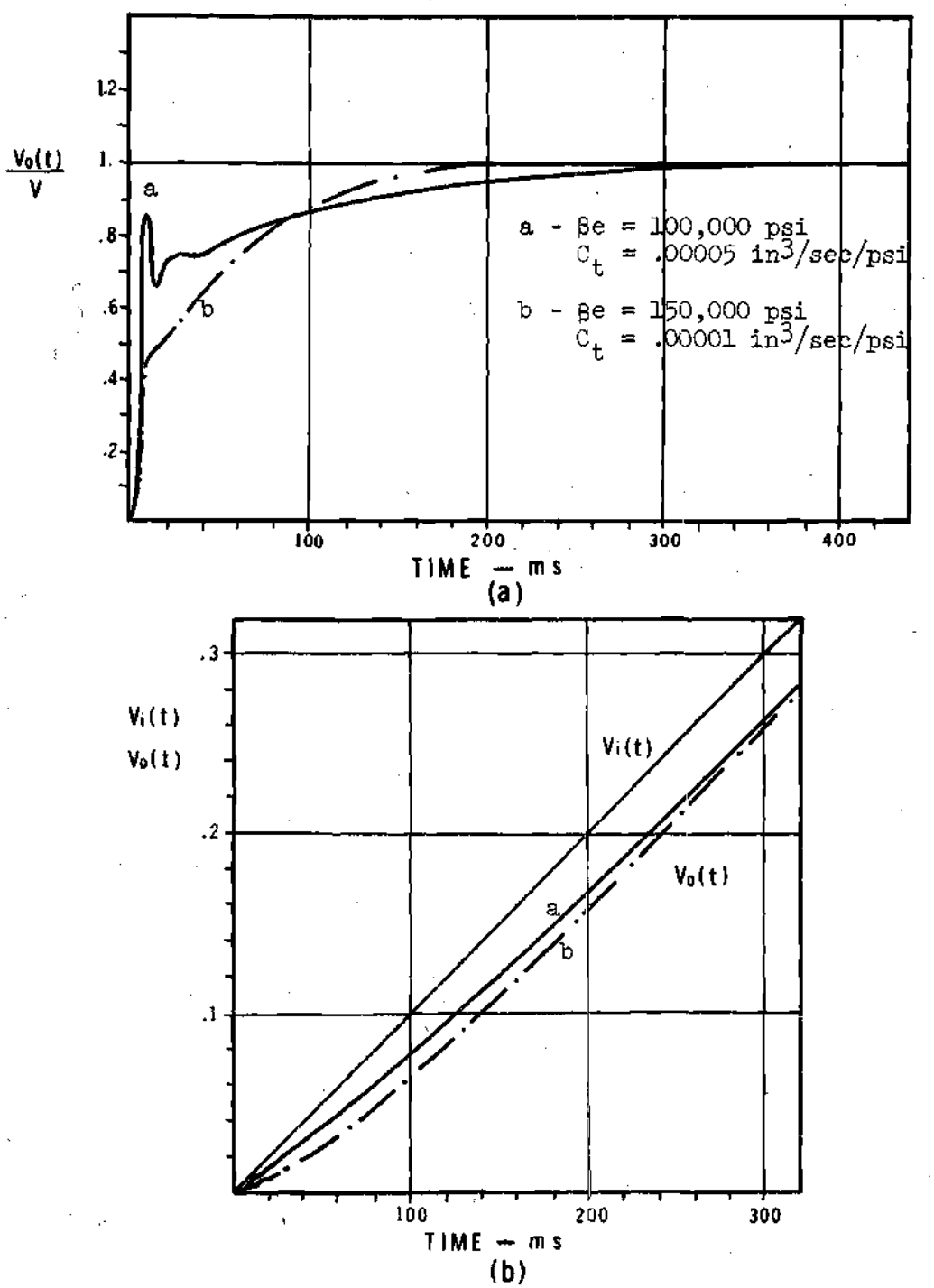

Figure 18. Transient Response for the Unloaded Position System with T_1 = .05 sec and T_2 = .0033 sec.
(a) Step Input
(b) Ramp Input.

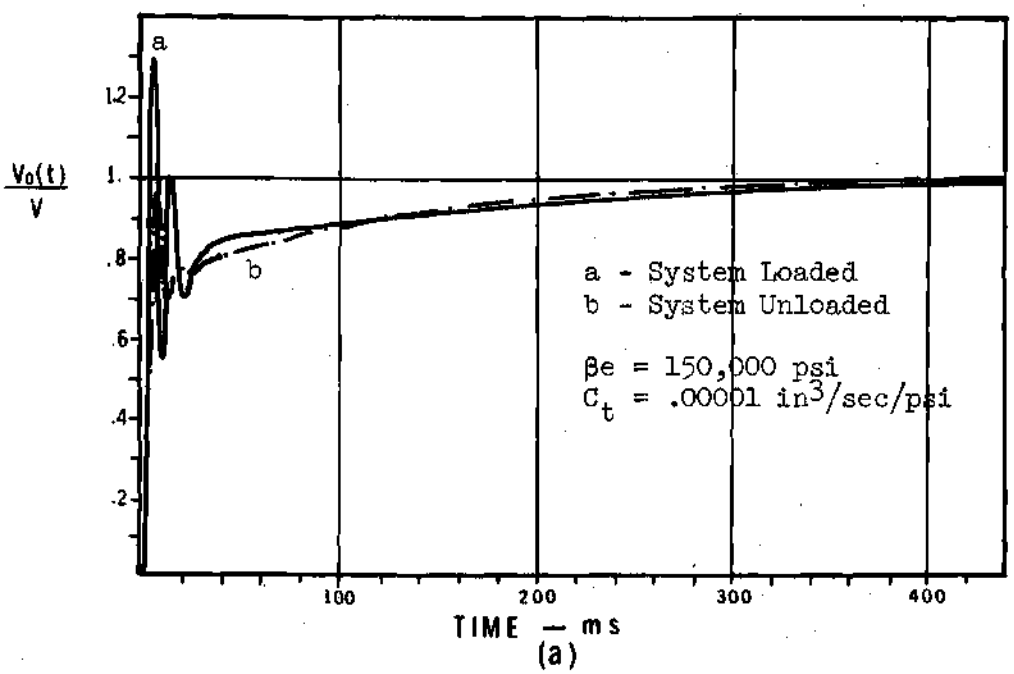

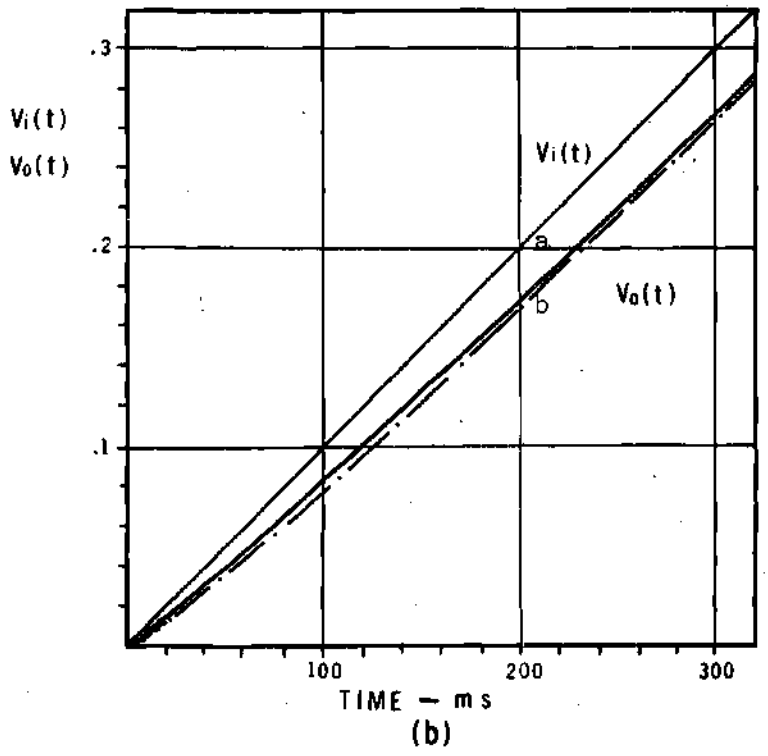

Figure 19. Transient Response for Displacement Output with T_1 = .1 sec and T_2 = .0033 sec
(a) Step Input
(b) Ramp Input.

E(s) = System's error signal, Volts

From Figure 7 it can be seen that

$$E(s) = \frac{Vi(s)}{1 + G_d(s)} \tag{39}$$

Considering a step input

$$Vi(s) = \frac{V}{s}$$

and subsitiuting in values and taking the limit on equation (39)

$$e_{ss}(t)_{\to\infty} = \frac{V}{1 + \frac{A^2KaK_tK_v}{K_1C_t}} \tag{40}$$

For no load or no leakage ($K_1 = C_t = 0$)

$$e_{ss} = 0$$

For load, $C_t = .00005$ $in^3/sec/psi$ and V = 10.V(max)

$$e_{ss} = 4.65 \times 10^{-3}V = .0118 \text{ mm}$$

If the system is loaded and $C_t = .00001$ $in^3/sec/psi$ for a maximum input (V = 10.V)

$$e_{ss} = 8.47 \times 10^{-4} V = .0025 \text{ mm}$$

As can be seen the steady state error depends on the load and total leakage coefficient in the piston.

Force Feedback Compensator

From Figure 12 and equation (18) it is evident that the instability of the system is due to the complex pair of poles produced by ω_h and ξ_h in combination with the real zeros due to the second order term

$$s^2 + 2\xi_f \omega_f s + \omega_f^2.$$

If this case is compared with the displacement feedback case everything indicates that the cancellation of the complex poles will stabilize the system and the two real zeros will act as the two lead-networks used before.

Introducing the same bridged-T network (Figure 13a) into the feed-forward path the pole cancellation is performed and the response of the system with force feedback should be stabilized. All the equations of the bridged-T network as well as the expressions for R, C_2 and C_3 are identical to those used for the case of displacement feedback.

System Response - Force Feedback

Frequency Response

With the compensating network included the open loop transfer function for the case of force feedback becomes

$$G_f(s) = \frac{L[s^2+2\xi_f\omega_f+\omega_f^2]\,[s^2+2\xi_h\omega_h s+\omega_h^2]}{[s^2+2\xi_v\omega_v s+\omega_v^2][s(s^2+2\xi_h\omega_h s+\omega_h^2)+B][s^2+2\xi_p\omega_h s+\omega_h^2]} \qquad (41)$$

and the closed loop one

$$H_f(s) = \frac{G_f(s)}{1+G_f(s)} \qquad (42)$$

Following the same procedure as before on the digital computer, the open and closed loop Bode plots are obtained and are shown in Figures 20 and 21. From Figure 20 it is readily seen that the system has a reasonable gain margin through 3,000 rad/sec., although there is a resonant peak that will make the transient response somewhat oscillatory. Figure 21 shows that the system is stable after the inclusion of the compensating network. Both Figures 20 and 21 show the influence of βe and C_t on the response.

Transient Response

If the same procedure as that used for the case of displacement feedback is applied here, the transient response of the system to step and ramp inputs is found to be as shown by Figure 22. Figure 22a

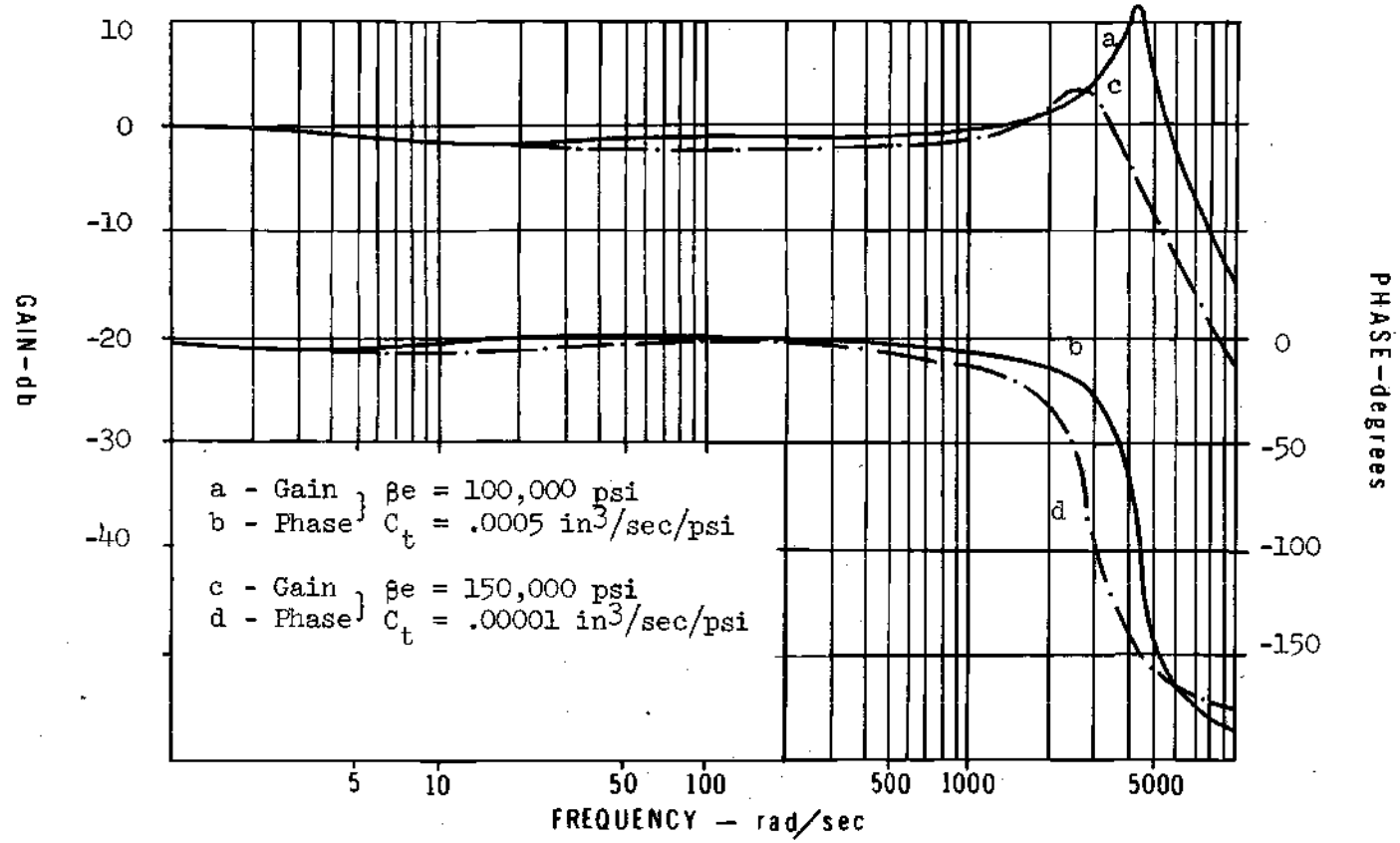

Figure 20. Compensated Closed-Loop Frequency Response Showing the Effect of Varying βe and C_t. Force Output.

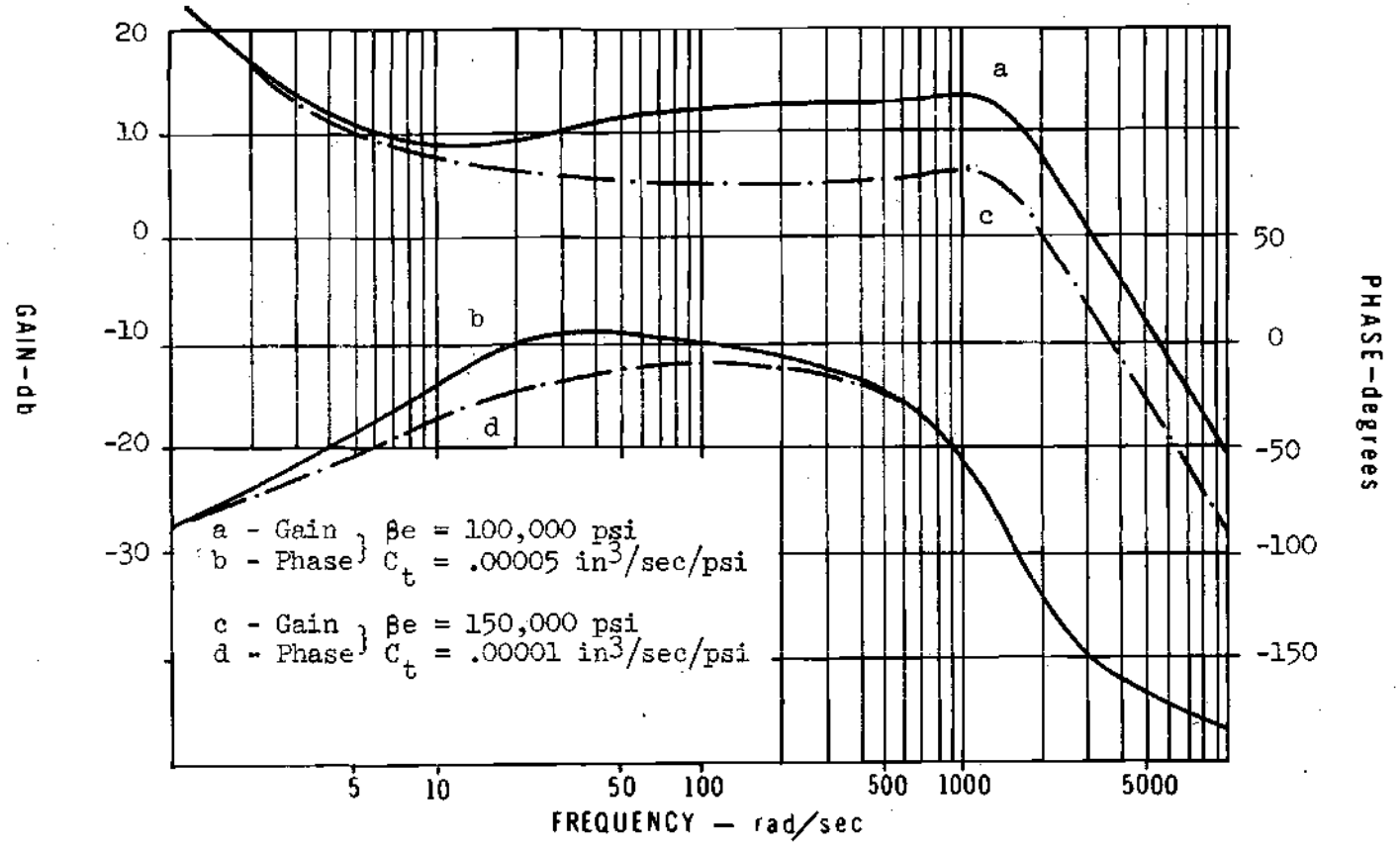

Figure 21. Compensated Open-Loop Frequency Response Showing the Effect of Varying βe and C_t. Force Output.

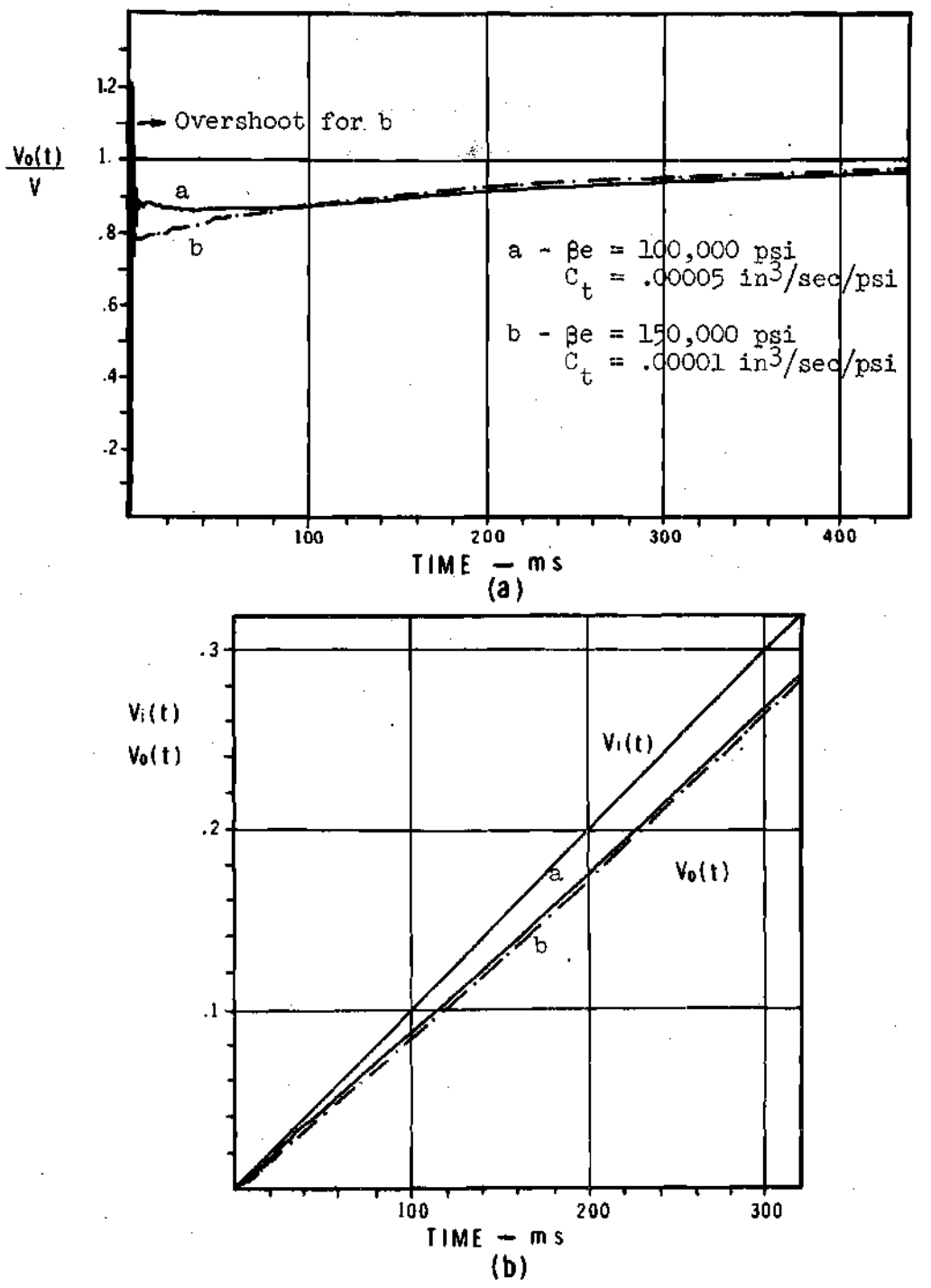

Figure 22. Transient Response for Force Output Showing the Effect of Varying βe and C_t.
(a) Step Input
(b) Ramp Input.

shows that the response oscillates and overshoots in the first 10 milliseconds and then goes smoothly to the steady state value. Figure 22b shows that the system will respond to a ramp input with some noise up to 30 milliseconds. In both cases the time to reach the steady state meets the specifications.

Steady State Error

The equation that represents the steady state error for a step input is, in this case,

$$e_{ss}(t)_{\to\infty} = \frac{V}{1 + \frac{A^2 K a K_{tf} K_v M_L \omega_f^2}{K_1 C_t}} \tag{43}$$

For $C_t = .00005$ in^3/sec/psi

$$e_{ss} = .005\ V = .5 \text{ grams}$$

For $C_t = .00001$ in^3/sec/psi

$$e_{ss} = .001\ V = .1 \text{ grams}$$

Summary of the Theoretical Approach

The analysis of the system has been done in Chapter II. From there it was found that the system needed compensation in both cases. In the case of displacement feedback two compensating networks have been introduced into the forward path of the closed loop: one to reduce the resonant peak and oscillations and the other to improve the

gain ratio. In the case of force feedback the system was unstable and the same bridged-T network used for the other case has been used to stabilize it.

The frequency and transient response analyses have been performed and the system has been found to meet the specifications. Table 3 gives a comparative analysis of the specifications with the predicted results. For all the situations the theoretical analysis shows that all specifications are met with a wide range left for the real system to vary from the predicted behavior.

Table 3. Specifications Compared with the Theoretical Predictions.

	Displacement Feedback		Force Feedback	
Item	Specifications	Predicted	Specifications	Predicted
Steady State Error	± .2%	< ±.04%	± .2%	< ±.05%
Rise Time*	.5 sec	< .2 sec	.5 sec	< .32 sec
Phase Shift	<180° @ 60cps	<120° @60cps	<180° @ 60cps	<20° @ 60cps
Gain Att.	<70% @ 60cps	<45% @60cps	<70% @ 60cps	<30%@ 60cps

* Rise time as defined by B. C. Kuo [27]

CHAPTER IV

EXPERIMENTAL PROGRAM

Once the system was designed, the components were obtained and assembled as shown in Figure 23.

Two kinds of experiments were carried out, to determine the system's response. The first one was made without load and with displacement as the controlled variable. Data were taken from the system, first without any compensation, secondly with the bridged-T network, and finally using both bridged-T and lead networks. This particular order permitted the adjustment of the resistances and capacitors of the compensator to their appropriate values.

The second set of tests were done using a cat muscle, in vivo, as the load. The cat was anesthetized and the hind limb was dissected in order to obtain access to the triceps surae muscle group for direct attachment to the force transducer. In this case both displacement and force were controlled (one at a time).

All system tests and analyses were carried out using frequency response data to be consistent with the theoretical approach presented in Chapters II and III. The frequency response data were obtained using the output of a sine wave generator as the input of the system. The amplitude and phase angle in the feedback path (output of the transducers). The readings were taken from the Lissajous pattern displayed on a storage oscilloscope (see Figure 23).

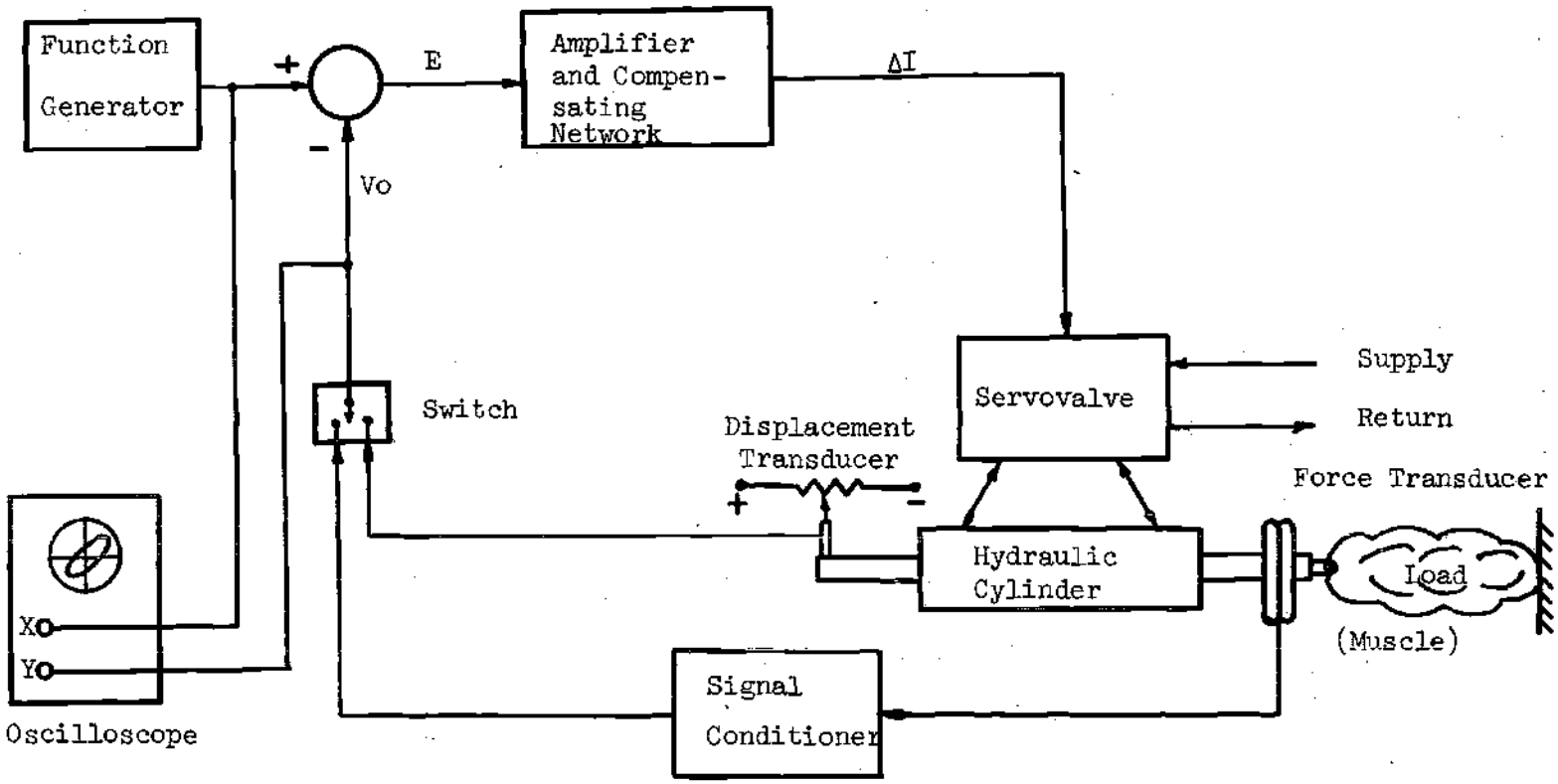

Figure 23. Diagram Showing the Arrangement Used in the Experiments.

The transient response of the system to both step and ramp inputs was also obtained. These data were derived from pictures taken from the storage oscilloscope display. The steady state error was measured from the response to a step input. All the tests were performed several times to observe the consistency of the results.

The information obtained is presented in the next chapter and then compared with the theoretical predictions. Finally the performance of the actual system is compared with the specifications.

CHAPTER V

COMPARISON OF THE THEORETICAL APPROACH AND THE EXPERIMENTAL RESULTS

System Under No-Load Condition

Only the case of displacement feedback was considered under no-load conditions since with force as the controlled variable the output of the system is always zero.

System Uncompensated

The experimental frequency response was obtained and the results plotted as curves a and b in Figure 24. In the same graph the theoretical closed loop Bode plot is presented for comparison. From these curves it can be seen that the actual system has a resonant peak at a lower frequency and its damping ratio is longer than was calculated in the theoretical approach. It also has a better gain ratio than the predicted.

These differences may be attributed to the facts that the real system has a larger actual leakage coefficient in the cylinder that was assumed, that the effect of the frictional forces which are actually present but were neglected in the analysis are considerable and that the system is not really linear as assumed.

System with Bridged-T Network

From the experimental Bode plot of the previous experiment, it was possible to adjust the values of the resistors (R) and the variable

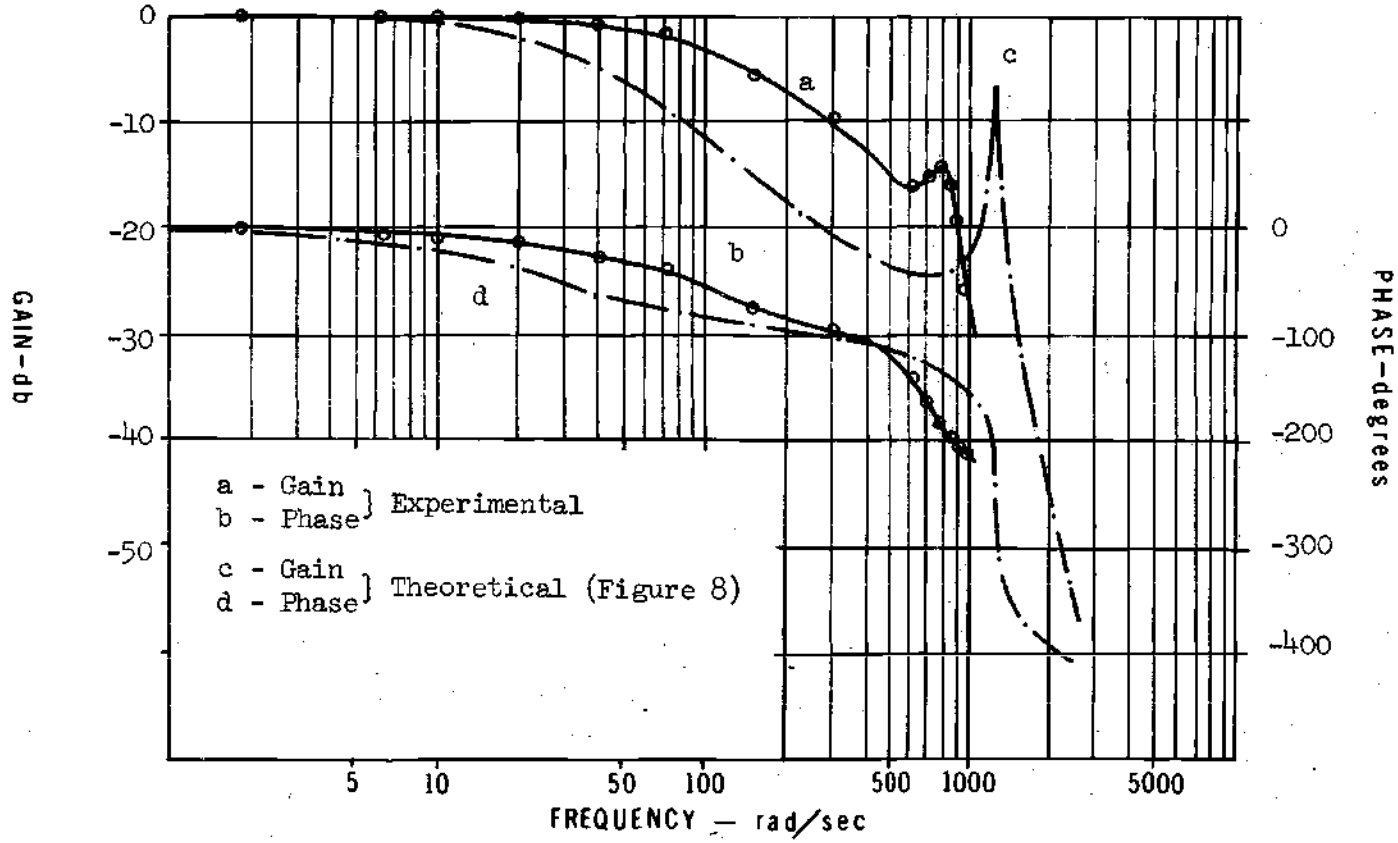

Figure 24. Closed-Loop Frequency Response Showing the Difference Between Theory and Experiments. Displacement Output without Compensation.

capacitor (C_2), to achieve the pole cancellation described in Chapter III. After this was done the experimental frequency response was obtained and the results, shown in Figure 25, are compared with the theoretical response, in the same figure.

With reference to Figure 25 it can be seen that the predicted and actual responses agree very closely.

System with Full Compensation

With the system constantly maintained in a stable region a compromise between transient and frequency response was achieved with the lead circuit. The time constants used were T_1 = .05 sec and T_2 = .0033 sec. Under these conditions both the frequency and transient responses were obtained experimentally, as described in Chapter IV.

Figure 26 shows both the experimental frequency response and the theoretical frequency response for comparison with the predictions of Chapter III. From these plots it is seen that the gain ratio and phase angle agree very closely with that predicted up to 300 rad/sec. After this point the experimental gain drops showing a difference with the analytical values. Part of this difference can be attributed to the fact that the operational amplifiers used in the compensating network did not have the high input impedance that was assumed in the design. This caused the gain of the system to be attenuated in the network. Nevertheless, the closed loop gain ratio was maintained within the specifications.

The results obtained for a step input are ploted and compared with the predicted response in Figure 27a. From there it can be seen

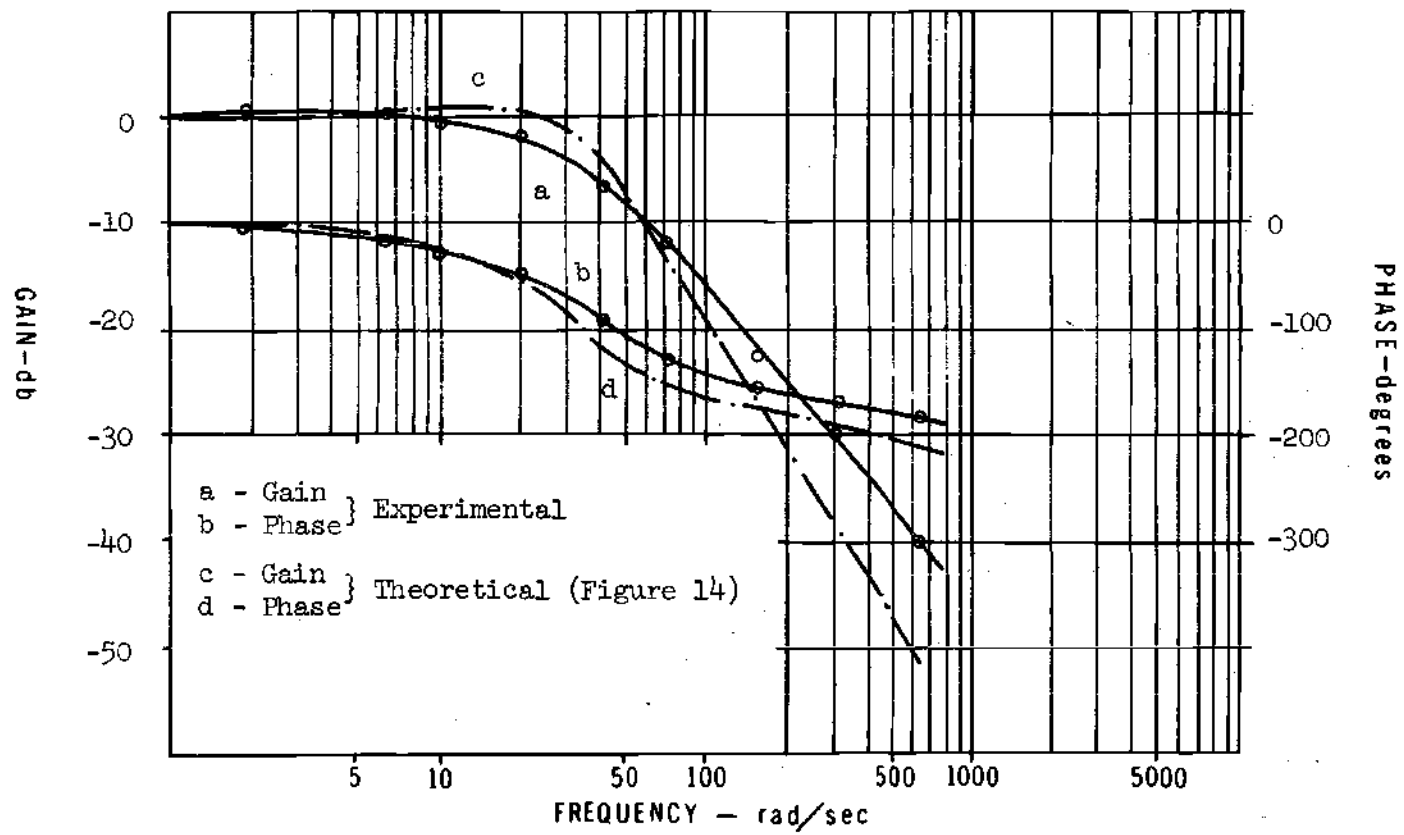

Figure 25. Experimental and Theoretical Frequency Response After the Inclusion of the Bridged-T Network. Displacement Output.

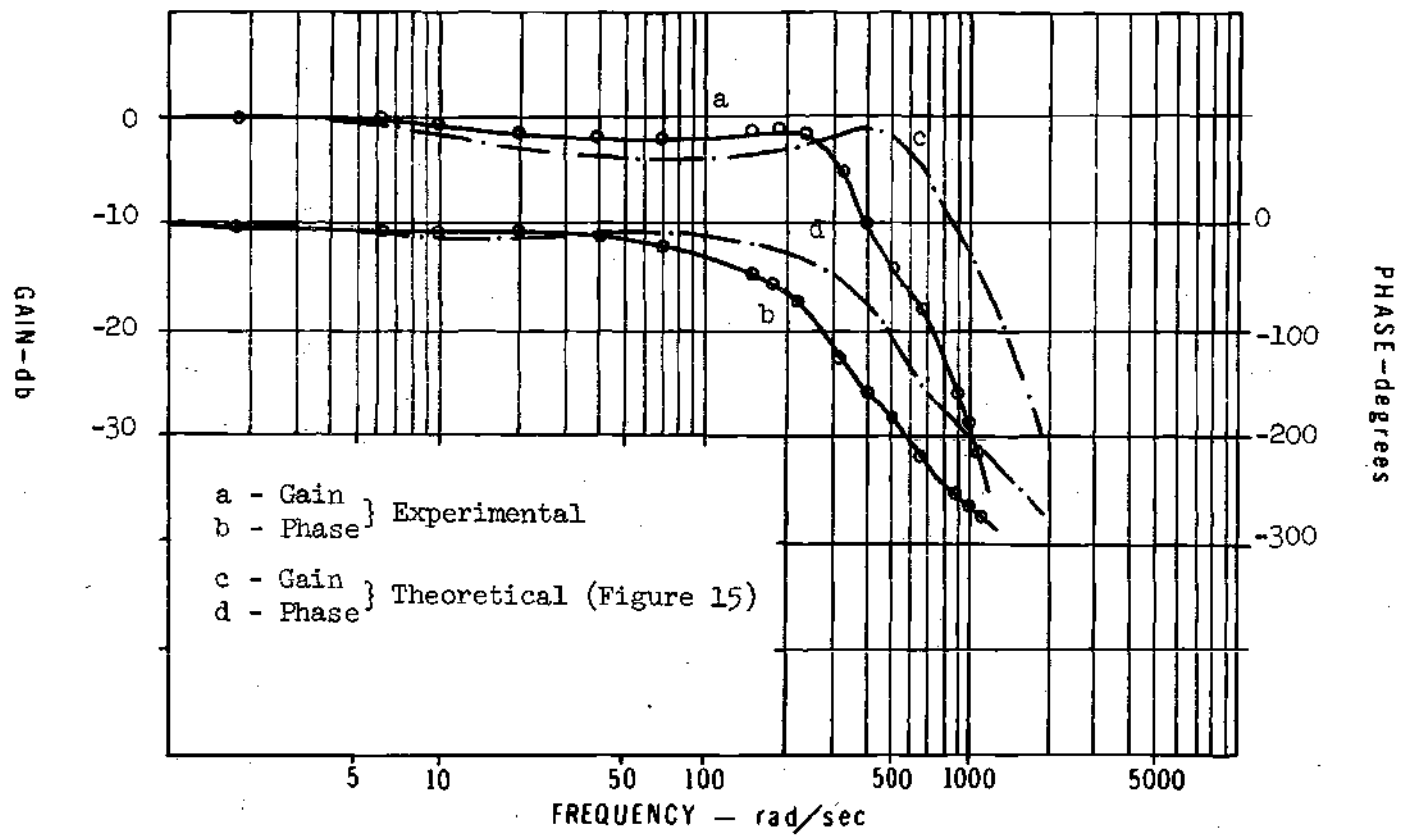

Figure 26. Experimental and Theoretical Frequency Response Using Full Compensation. Displacement Output without Load.

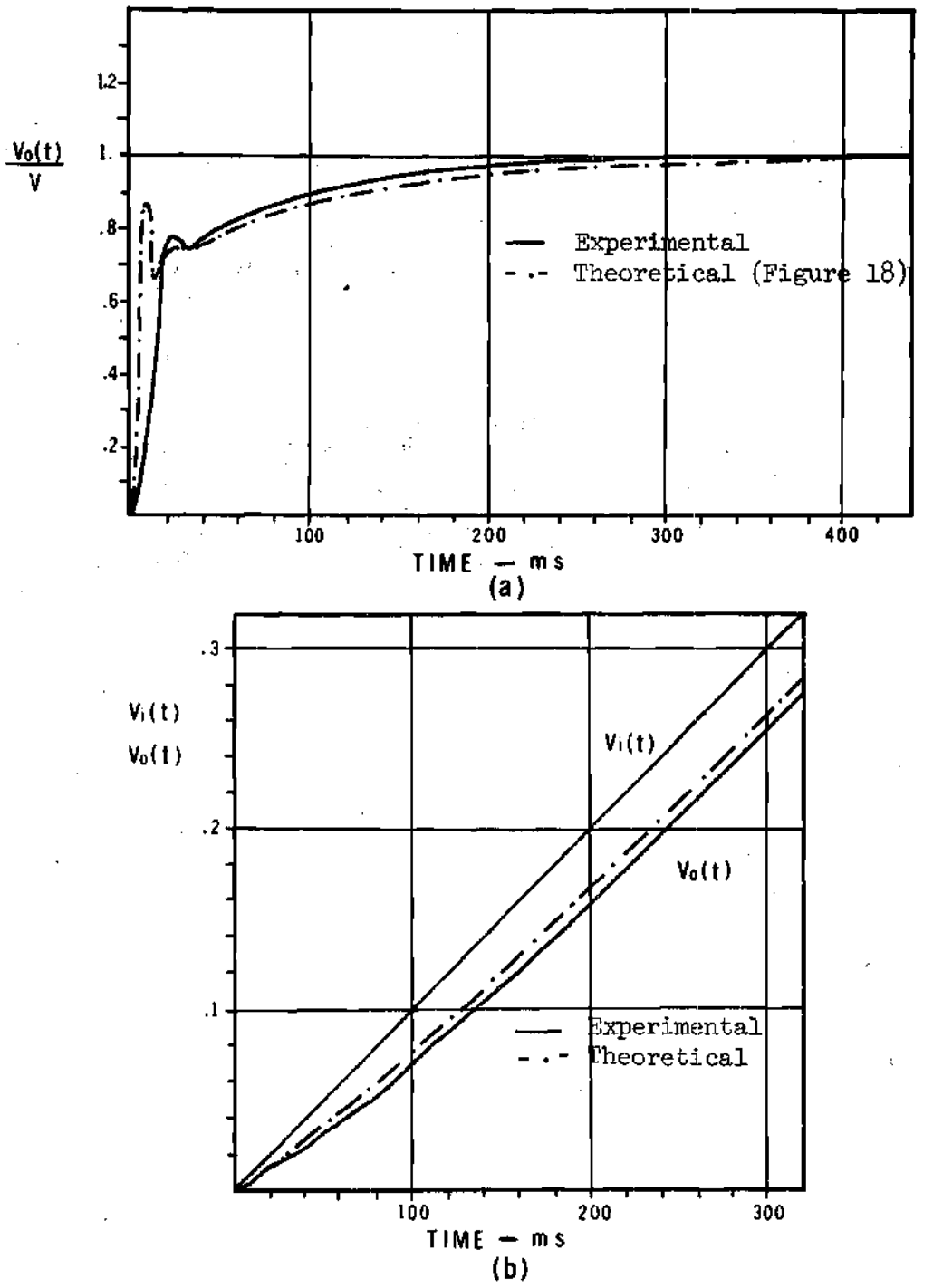

Figure 27. Experimental and Theoretical Transient Response. Displacement Output without Load.
(a) Step Input
(b) Ramp Input.

that both the theoretical and the experimental responses follow the same pattern. The latter is more damped and has a smaller rise time. From the same graph the steady state error was found to be too small to be perceived. Figure 27b shows the difference between theory and experiment for the response of the system to a ramp input. From there it is seen that the responses agree in the first 25 milliseconds. After this, both follow the same pattern with a difference of less than 1 percent and the error is slightly larger in the real system.

System Loaded

With a cat muscle as the load the experimental frequency and transient responses were obtained again. Tests with displacement and force feedback were carried out and the results are reported below.

Displacement Feedback

Data were obtained with the same parameters used in the unloaded condition.

The results obtained for this case, with displacement as the controlled variable, were the same as in the unloaded case. No appreciable difference was found.

Force Feedback

With force as the controlled variable, the experimental frequency and transient response of the system was obtained for two different situations. In the first, the tests were done with an active muscle, that is with the peripheral nerve intact. This permitted the muscle to contract due to the stretch reflex loop. After these experiments were performed, the nerve was cut and a

second set of data were taken. In this case the muscle acted passively, meaning that no contractions were present and its behavior was more like a purely passive mechanical system. The results corresponding to both cases are presented next.

Figure 28 shown both the frequency response obtained for an active muscle and that predicted in Chapter III. A reasonable agreement is found up to 400 rad/sec. At this point the experimental response breaks down with a resonant peak at approximately 1,250 rad/sec. The predicted value of this peak was 2,500 rad/sec. The main reason for this difference is the mathematical model used for the muscle, which apparently is far from being a good one. The low input impedance of the operational amplifiers used in the compensating network may be an additional factor.

It is interesting to note that when the system was run without the bridged-T compensating network it became unstable as predicted.

Figure 29 shows the response of the system with the passive muscle load, that is, with the muscle nerve cut. The main difference of this response compared with the case of Figure 28, is that the gain drops down at lower frequency. The resonant peak is also smaller meaning that its damping ratio is bigger.

The difference between the response for an active and passive muscle was noticed by N. P. Rosenthal, et al [5] and is attributed to the dynamic characteristics of the active muscle when the stretch reflex is intact.

The response to a step input is presented in Figure 30a. Curve a is the response obtained experimentally with an active muscle as the

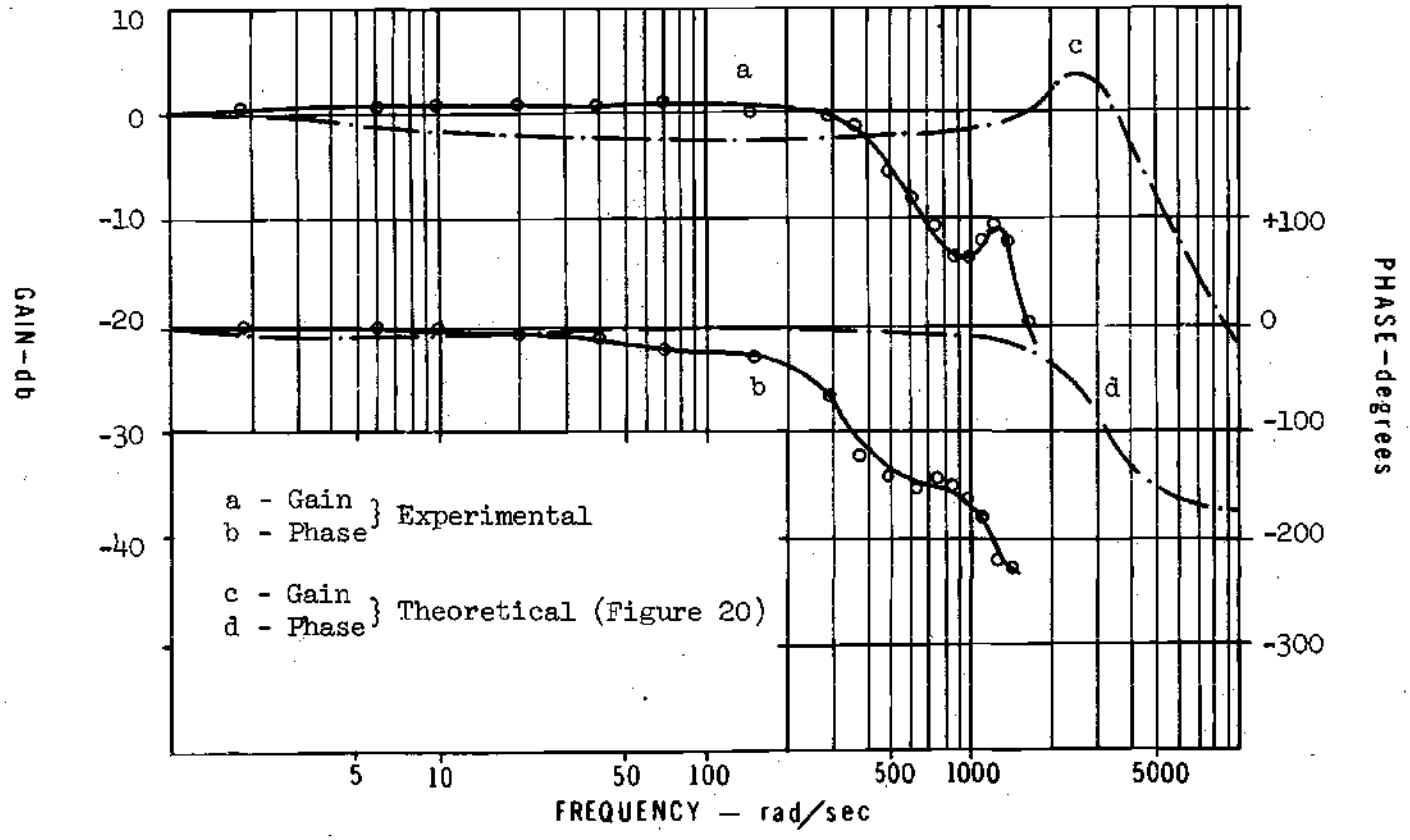

Figure 28. Experimental and Theoretical Frequency Response for an Active Muscle. Force Output.

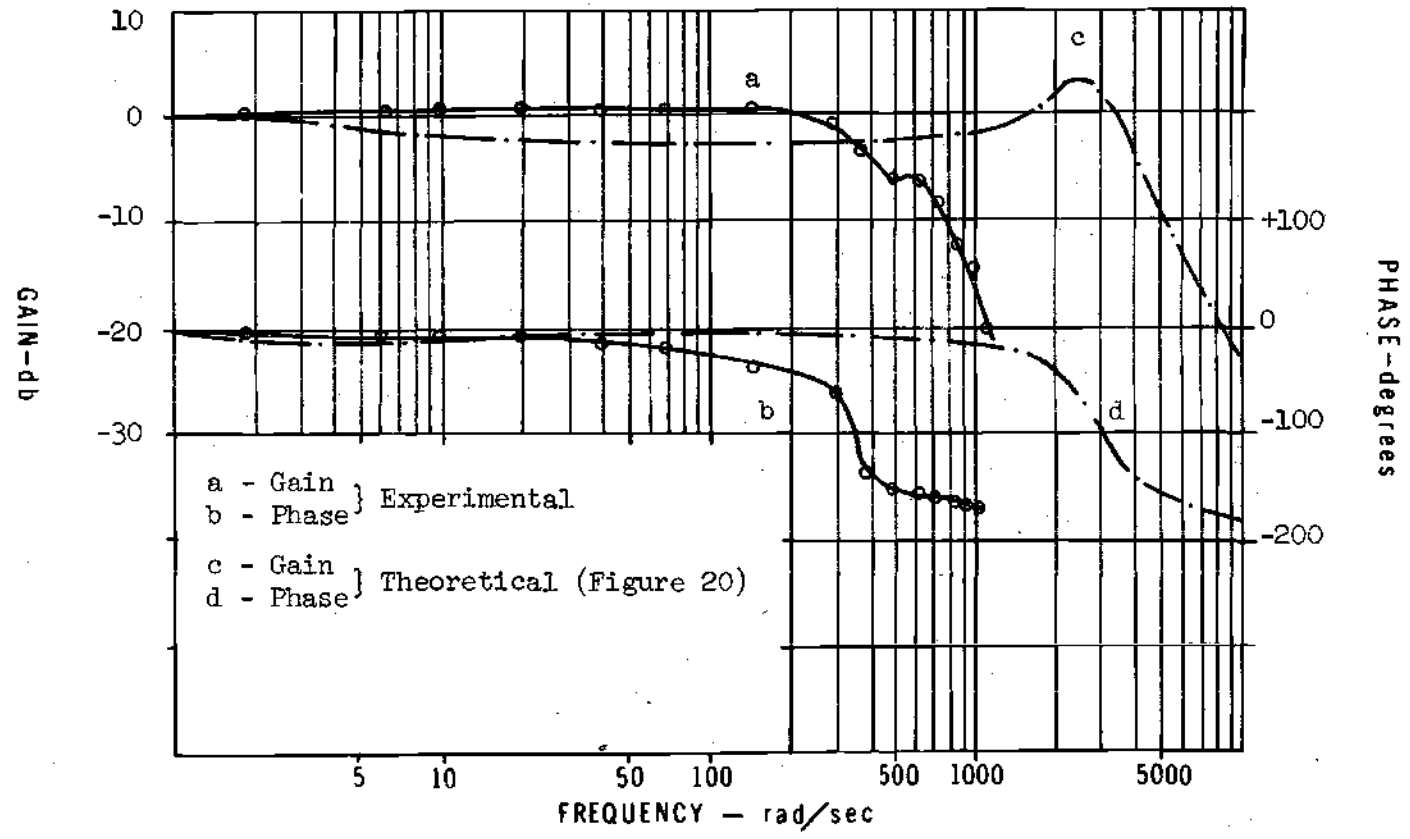

Figure 29. Experimental and Theoretical Frequency Response for a Passive Muscle. Force Output.

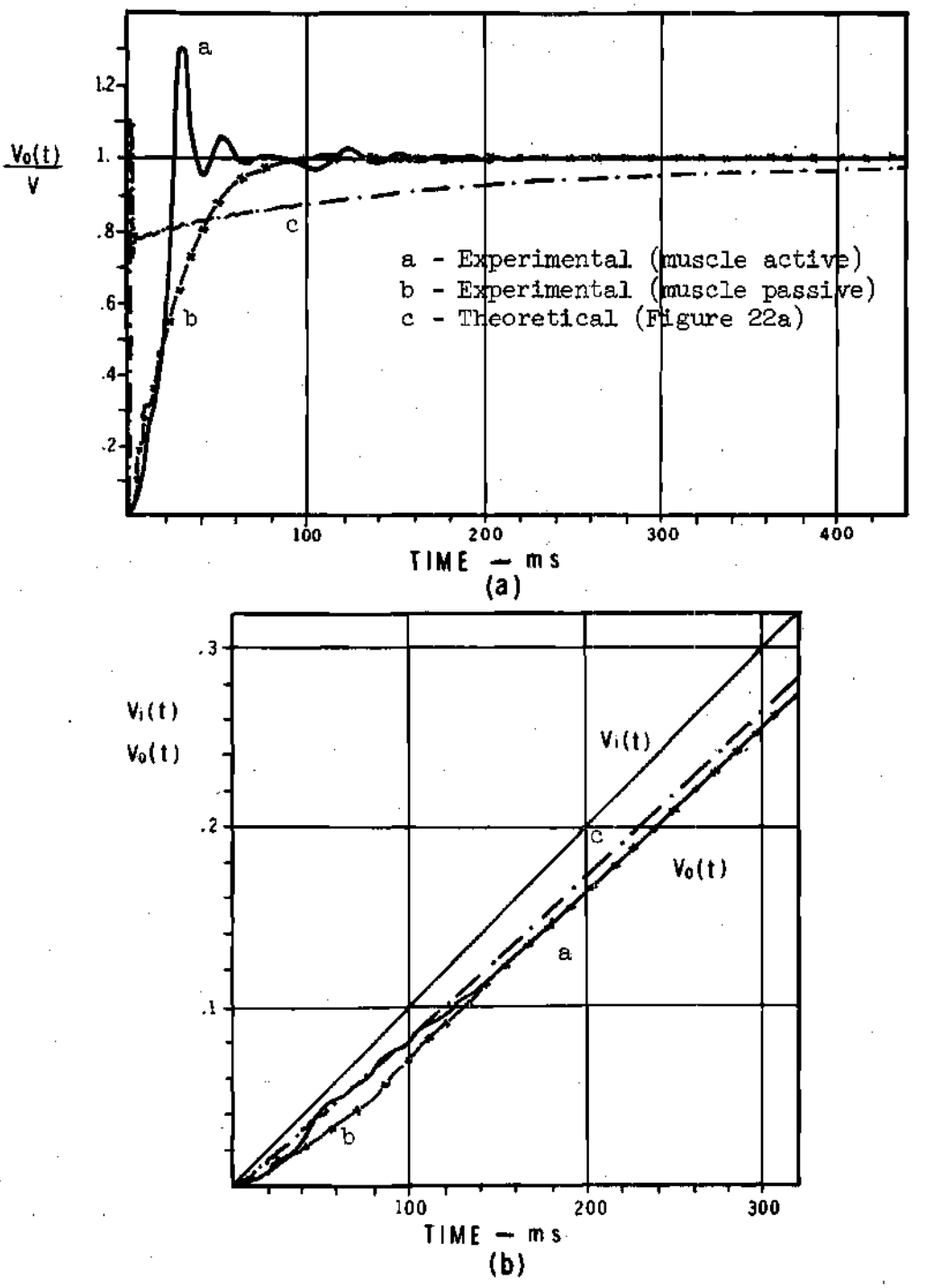

Figure 30. Experimental and Theoretical Transient Response for Force Output.
(a) Step Input
(b) Ramp Input.

load. The comparison of this response with the theoretical (curve c) tells us that the rise time is smaller than was predicted and there is not good agreement between them. Again, this shows that the model used for the muscle is not appropriate.

Curve b shows the data obtained for the same muscle in a passive state, i.e., with the nerve cut. Comparison with the case where the nerve was intact showed that the response is smoother for the passive muscle. This was expected, as from the frequency response, it was seen that a bigger damping ratio acted in this case. Furthermore, with the nerve cut, the muscle could no longer help attain the final value of force by generating tension. Finally, the response to a ramp input is presented in Figure 30b. Curves a and b correspond to the experiments for an active and inactive muscle, respectively. Compared with the theoretical approach both responses are noisier in the first 120 milliseconds and follow the same pattern after that. There is also a difference of about 1 percent once the steady state is reached.

When the transient response was studied experimentally, it was found that the behavior of the muscle is non-symmetrical. That is, the responses were different when the steps imposed as the input were applied in opposite directions. This can be seen from observation of Figure 31 which presents the responses to a step input from zero to 500 grams and from 500 to zero grams. From here it can be noticed that the muscle behavior is nonlinear.

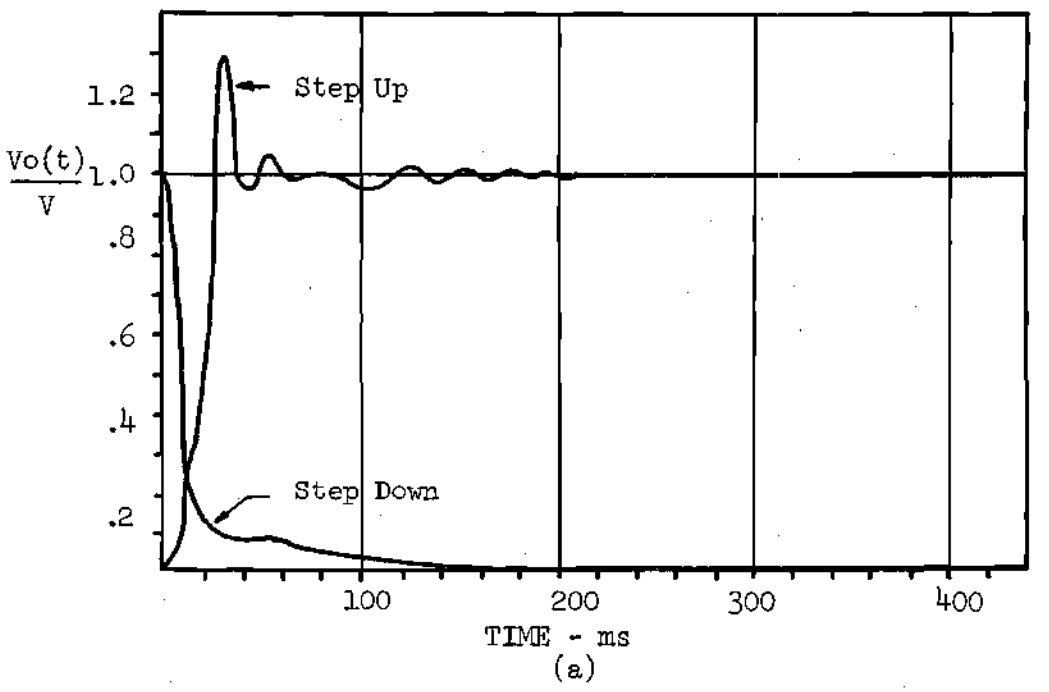

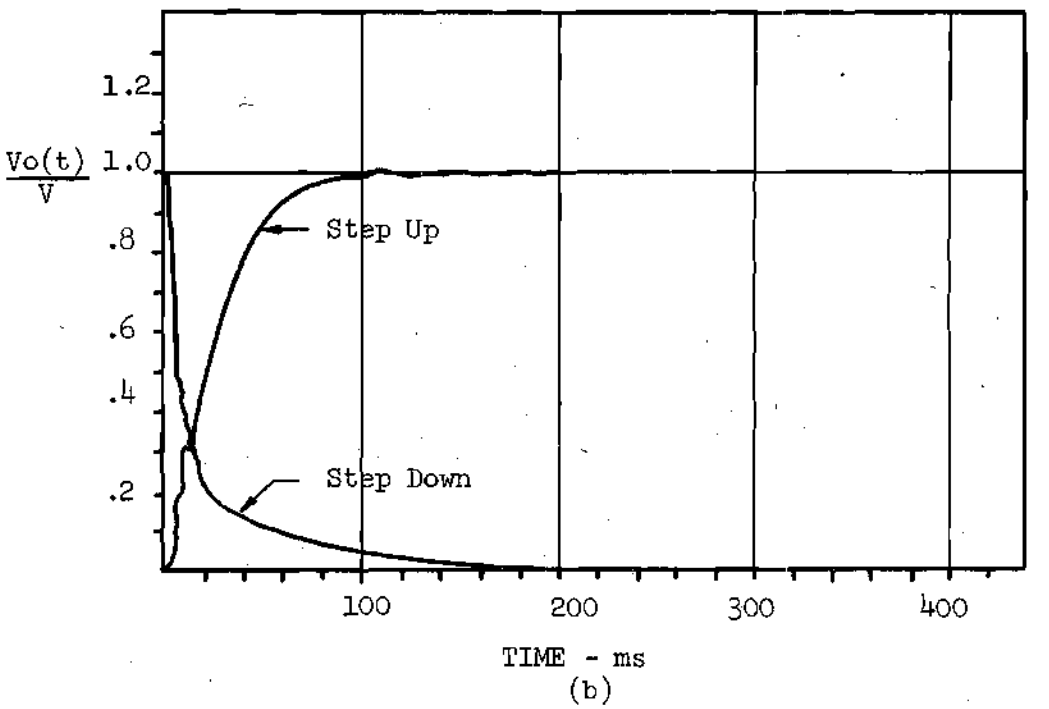

Figure 31. Experimental Response Showing Non-Linearity:
(a) Muscle Active
(b) Muscle Passive.

Specifications and the Actual System

The experimental analysis performed, with force and displacement as the controlled variables, show that the specifications imposed on the system have been met for both cases.

Table 4 gives a comparative scheme for the control requirements. The measurement specifications were also met and the components (transducers) to achieve them are described in Appendix II.

Table 4. Specifications Compared with the Actual System.

	Displacement Feedback		Force Feedback	
Item	Specifications	Actual System	Specifications	Actual System
Steady State Error	± .2%	Not Appreciable	± .2%	Not Appreciable
Rise Time	.5 sec	< .160sec	.5 sec	< .070sec
Phase Shift	<180° @ 60cps	<150°@ 60cps	<180°@ 60cpa	<130°@ 60cps
Gain Att.	<70% @60cps	<65% @60cps	<70%@ 60cps	<40% @60cps

CHAPTER VI

CONCLUSIONS

From the analysis of the experimental data obtained and its comparison with the analytical model used for the design of the system, several conclusions may be drawn:

(1) The linear analysis of an electrohydraulic control system is a powerful tool for the prediction of its response within an acceptable margin of approximation.

(2) The response of the system is limited by the dynamic characteristics of the hydraulic cylinder and load.

(3) For the real position system designed the hydraulic damping ratio is bigger than that obtained from the linear computations.

(4) When force is controlled the response of the system is strongly dependent on the dynamics of the load.

(5) Muscles behave in a very nonlinear fashion. This is more noticeable when the nerve is intact and the stretch reflex is working.

(6) The apparent damping ratio of the muscle increases when it is passive, compared with the active situation.

CHAPTER VII

RECOMMENDATIONS

Two recommendations may be given for the improvement of the actual system and further study in the design of this class of devices.

The response of the system could be imporved by introducing operational amplifiers with the highest input impedance available in the compensating network. This would permit a better adjustment of the compensating network and eliminate some gain drop in the system. It is difficult to predict the improvement that can be achieved with this alteration, but some should be obtained as there are saturation problems when the gain drop caused by the low input impedance is compensated using bigger gains in the amplifiers of the lead circuit.

If further research has to be done in the design of this class of devices, and expecially for force control, it is important to assume a more complex model for the dynamic representation of the muscle. This will permit a better approximation between predictions and experiments and a better system should result. The use of a distributed parameter model would probably offer a much better prediction of behavior.

APPENDIX I

MUSCLE CONSTANTS

The mechanical model of the muscle was assumed to be of the form described by equation (11) and shown in Figure 6, Chapter II.

In order to estimate the values of M_L, K_1 and C some experiments were performed. Static forces were applied to the triceps surae muscle group of a cat, in vivo, and the displacements produced by the forces were measured. The results were plotted, as shown in Figure 32. From this plot the average slope of the curve was taken as the linearized spring constant, K_1.

$$K_1 = 33.333 \text{ grams/mm} = 1.86 \text{ lb/in}..$$

The value for muscle mass (M_L) was approximated with the largest muscle to which the system will be applied (about .55 lb). Therefore,

$$M_L = \frac{\text{weight of muscle}}{\text{acc. of gravity}} = \frac{.55 \text{ lb}}{3.22 \text{ in/sec}^2} = .01695 \text{ lb sec}^2/\text{in}$$

Finally, the muscle was assumed to be overdamped ($\zeta_f = 1.2$). Therefore, rewriting equation (11) equal to zero

$$M_L s^2 X(s) + C s X(s) + K_1 X(s) = 0$$

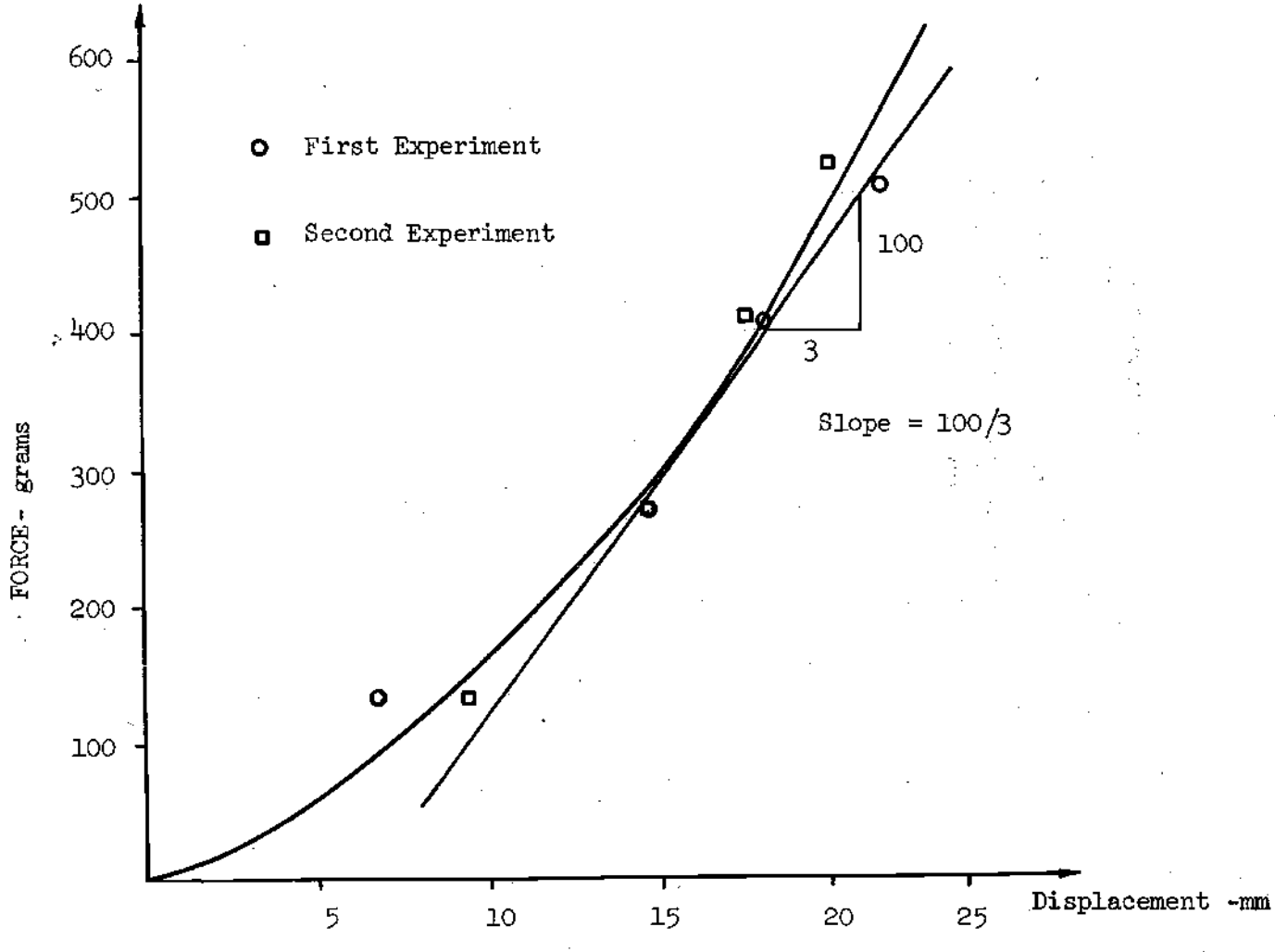

Figure 32. Force Versus Distance Stretched.

From this equation

$$\omega_f = (K_1/M_L)^{\frac{1}{2}}$$

$$\xi_f = C/2\ M_L\omega_f$$

and from there

$$C = 2\xi_f(K_1M_L)^{\frac{1}{2}}$$

Substituting in values

$$\omega_f = 10.475 \text{ rad/sec}$$

$$\xi_f = 1.2 \text{ (assumed)}$$

$$C = (.2)(1.2)[(1.86)(.01695)]$$

$$C = .425 \text{ lb sec/in}$$

APPENDIX II

SELECTION OF COMPONENTS AND EVALUATION OF PARAMETERS

Transducers

Force

To meet the specifications it was required to measure from 0 to 10,000 grams with readings of .5 to 1.0 gram. This was not possible due to the extremely high resolution required. The problem was solved by using a transducer with a range of 0 to 1,000 grams and leaving the possibility of using an alternate transducer ranging from 0 to 10,000 grams of lower resolution. This was permitted due to the fact that the experiments would never need to go through the extreme values in the same run. Both design and experiments were performed on the basis of the lower range.

The characteristics of the transducer and amplifier/conditioner are as follows:

Transducer:

Capacity: 0 - 1,000 grams

Type: Strain gage - Wheatstone Bridge

Input voltage: 10 volt

Output voltage: 2 millivolt/volt

Amplifier/Conditioner:

Gain: 20 to 500

Output voltage: Continuously adjustable from 0 to $\pm$ 10 V DC

Thus, using a supply of 10 V DC for the transducer, the amplifier gives a ± 10 V DC output. So, the transducer/amplifier gain (K_{tf}) is

$$K_{tf} = \frac{10 \text{ Volt}}{1{,}000 \text{ grams}} = 10^{-2} \frac{\text{Volt}}{\text{gram}} = 4.535 \text{ V/lb}$$

This means that each tenth of a gram is represented by 1 mV, which is measurable.

Displacement

For the displacement measurement a linear motion potentiometer was used, with the following characteristics was used

Range: 0 - 25.40 mm(1.0 in)

Input: ± 10 V DC

Output: 0 - ± 10 V DC

Resolution: Continuous (conductive plastic)

So, the potentiometer constant (K_t) is

$$K_t = \frac{10 \text{ V}}{25.40 \text{ mm}} = .3937 \frac{\text{V}}{\text{mm}} = 10 \frac{\text{V}}{\text{in}}$$

Therefore, each tenth of a millimeter is represented by 39.37 mV, which exceeds the specifications.

Hydraulic Cylinder

The combination of equations (10) and (11) yields

$$AP_L = (M_p + M_L)s^2 X(s) + C s X(s) + K_1 X(s)$$

The left hand member of this equation is the force that the piston applies to overcome the load reaction for given values of velocity (s X(s)) and acceleration ($s^2X(s)$).

A cylinder with .2 in^2 of affected area is selected*, the mass of the rod and piston is equal to .0061 lb-sec^2/in. The weight of the force transducer and the potentiometer rod is approximately .22 lb. so their mass is

$$M_{transducers} = \frac{.22 \text{ lb}}{32.2 \text{ in}^3/\text{sec}} = .00684 \text{ lb sec}^2/\text{in}$$

So,

$$M_p = .01294 \text{ lb-sec}^2/\text{in}$$

and

$$M = M_L + M_p = .02989 \text{ lb-sec}^2/\text{in}$$

The typical maximum velocity and acceleration required by the experiments are

$$s^2X = 5.5 \times 10^3 \text{ in/sec}^2$$

$$sX = 5.5 \text{ in/sec}$$

* Clippard Minimatic, model HgD, with maximum working pressure of 2,000 psi and 1 inch displacement.

If the maximum velocity and acceleration are assumed to occur simultaneously [22]

$$A\,P_L = (.01294)(5.5 \times 10^3) + (.425)(5.5) + (1.86)(1)$$

$$A\,P_L = 155.61 \text{ lb}$$

Thus,

$$P_L \geq \frac{155.61}{.2} = 778.05 \text{ psi}$$

The P_L selected was

$$P_L = 1{,}000 \text{ psi}$$

Finally the hydraulic natural frequency (ω_h) must be checked to be greater than 100 cps: then the values of A and P_L are not a limiting factor in the system's response

$$\omega_h = \left[\frac{4\beta e A^2 + 4C_t \beta e + V_t K_1}{V_t M}\right]^{1/2}$$

If,

$$V_t = \text{Vol. cylinder} + \text{vol pipes} = (.2)(1.0) + \frac{(3.14)(.12)^2(12)}{4}$$

$V_t = .34 \text{ in}^3$

$C_t = 0$ (which gives a lower ω_h)

$\beta e = 10^5$ psi

$$\omega_h = \left[\frac{(4)(10^5) + (.34)(1.86)}{(.34)(.02984)}\right] = 1{,}255.1 \text{ rad/sec}$$

$$= 200 \text{ cps}$$

Since $\omega_h \simeq 200$ cps will not limit the response of the system, the A and P_L of the selected cylinder are sufficient to meet specifications.

Servovalve

Equation (9) gives the flow into the cylinder as

$$Q_L(s) = A\, s\, X(s) + C_t\, P_L + \frac{V_t}{4\beta e}\, s\, P_L$$

Neglecting the last two terms of this equation

$$Q_L(s) = A\, s\, X(s)$$

Substituting in the values of area and velocity

$$Q_{L\,max} = (.2)\,(5.5) = 1.10 \text{ in}^3/\text{sec} = .285 \text{ gpm}$$

If a value with square root type pressure flow curves is assumed

$$Q_R = Q_L \left[\frac{P_L}{P_s - P_L}\right]^{1/2}$$

where

Q_R = Rated flow

$P_s = 3/2\ P_L$ = Supply pressure, psi

Then

$$Q_R = .285 \left[\frac{1000}{1500-1000}\right]^{1/2}$$

$Q_R = .403$ gpm at 1000 psi pressure drop

A two-stage, four-way, mechanical feedback, electrohydraulic servovalve with the following characteristics was selected

Supply pressure: 1,500 psi

Rated flow: .99 gpm at 1000 psi drop

1.4 gpm at 1,500 psi drop

Linearity: < 7 percent

Pressure-flow characteristics: see Figure 33a

Rated current: 10 mA, differential

Flow gain (Kv): .55 in^3/sec/mA

Frequency response:* see Figure 33b

Apparent natural frequency:* ω_v = 1,450 rad/sec

Apparent damping ratio:* ξ_v = .55

---

* Without dither

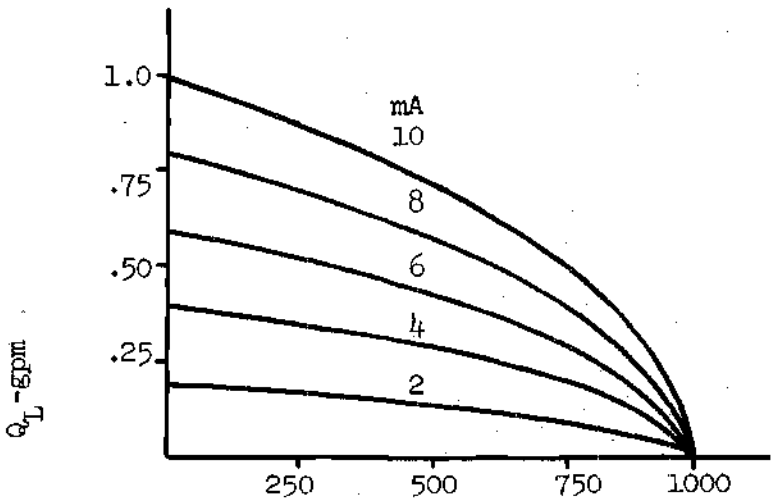

(a)

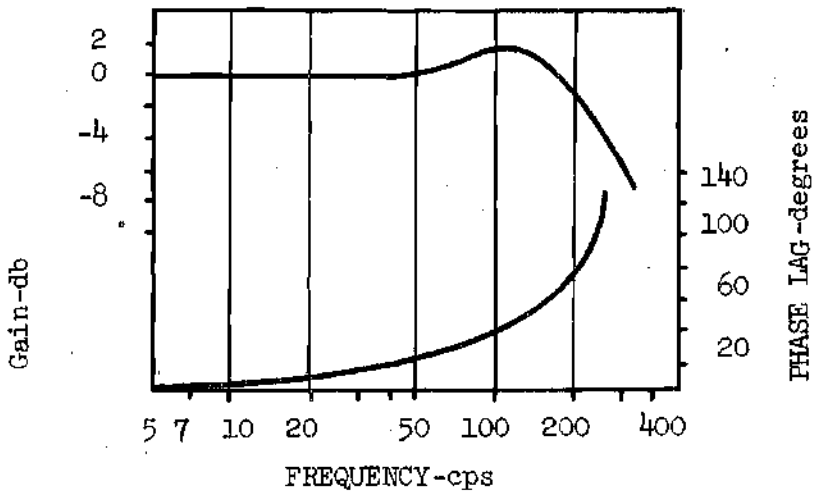

(b)

Figure 33. Servovalve Characteristics
(a) Pressure-Flow Characteristics
(b) Frequency Response

Electronic Amplifier

The amplifier used had the following specifications:

Gain (Ka): 1.0 mA/V

Gain linearity: $\pm$ 3 percent

Dead band: None

Frequency response: less than 3 db at 800 cps

Dither: Square wave, 20 to 300 Hz and 0 - 20 V pp

From the characteristics of all the components and the values of the effective bulk modulus (βe) and total leakage coefficient (C_t), that were discussed in Chapter II, a list of all the calculated parameters is given below for convenience in reference.

$Ka = 1.0$ mA/V

$K_t = 10.0$ V/in

$K_{tf} = 4.535$ V/lb

$Kv = .55$ in^3/sec/mA

$\omega_v = 1{,}450$ rad/sec

$\xi_v = .55$

$\beta e = 10^5$ to 1.5×10^5 psi

$C_t = .00001$ to $.00005$ in^3/sec/psi

$A = .2$ in^2

$C = .425$ lb-sec/in

$K_1 = 1.86$ lb/in

$M_L = .01695$ lb-sec^2/in

$M_p = .01294$ lb-sec^2/in

$M = .02989$ lb-sec^2/in

$V_t = .34 \text{ in}^3$

$\omega_f = 10.475 \text{ rad/sec}$

$\xi_f = 1.2$

APPENDIX III

COMPUTER PROGRAMS

Four main computer programs were used to get the Bode plots and transient response graphs of Chapters II and III. In the next pages a list of each of them is given.

The first program, labelled "Thesis BP" was used to produce Figures 8 to 11 and 14 to 17. Given the parameters of the system (line 6), the program calculates the open and closed loop Bode plots, some points of interest (ω_h, ξ_h, etc.) and also the values of R, R_1, R_2, C_1, C_2 and C_3.

The second program labelled "Thesis F" does the same as the first but for force feedback. Figures 12, 13, 20 and 21 were produced from it.

The third program labelled "Tre One" was used for Figures 18 and 19. It calculates the poles and zeros of the closed loop transfer function for displacement feedback and then gives the transient response for a step and ramp input. The data to be used are the same as for the first and second programs.

Finally, the last program labelled "Force One" performs the same as the third but for the case where force is the controlled variable. This was used to obtain Figure 22.

```
&LET,S1 CORRAL-F-J*THESIS,dP,,,1064470737lu
      BODE PLOT FOR OPEN AND CLOSED LOOP TRANSFER FUNCTION-DISPLACEMENT
      REAL K,KA,KT,KV,KL,WH,WV,DRH,DRV,BE,A1,CT,C1,VT,K1,
     1 W,PHASE,GAIN,M,MT,A,B,C,D,E,ABSVAL,GAINC,AESC,PHASEC,
     2 T1,T2,FIL
      COMPLEX G,GC,D1,D2,D3,D4,D5,D6,N1,N2,N3,D7,D8
      READ(5,7)KA,KT,KV,WV,DRV,BE,A1,CT,C1,VT,K1,MT,T1,T2,FIL
    7 FORMAT()
      WRITE(6,9) CT,K1,T1,T2
    9 FORMAT(4H CT=,F8.6,2X,3HA1=,F8.6,2X,3HT1=,F8.6,2X,3HT2=,F8.6,/)
      M=4.*BE*(A1**2)+4.*CT*C1*BE+VT*K1
      KL=(4.*BE*A1)/M
      WH=SQRT(M/(VT*MT))
      DRH=2.*CT*BE*SQRT(MT/(VT*M))+(C1/2.)*SQRT(VT/(MT*M))
      K=KA*KV*KT*KL*(WV**2)*(WH**2)
      A=2.*DRV*WV
      B=WV**2
      C=2.*DRH*WH
      D=WH**2
      E=(KL*(WH**2)*K1*CT)/(A1**2)
      DRP=(1.+2.*(DRH**2))/(2.*DRH)
      F=2.*DRP*WH
      WRITE(6,10)A,B,C,D,E,F
   10 FORMAT(4H A = ,F21.4,/4H B = ,F21.4,/4H C = ,F21.4,/
     1 4H D = ,F21.4,/4H E = ,F21.4,/4H F = ,F21.4)
      WRITE(6,19)KL,K,WH,DRH
   19 FORMAT(5H KL = ,F20.4,/4H K = ,F21.4,/5H WH = ,F20.4,/6H DRH =
     1 ,F19.4,//16X,9HOPEN LOOP,21X,11HCLOSED LOOP,13X//
     2 7H       W,9X,4HGAIN,6X,5HPHASE,6X,7HABSVALC,7X,
     3 5HGAINC,6X,6HPHASEC/10H   RAD/SEC,7X,2HDB,10X,3HDEG,
     4 22X,2HDB,10X,3HDEG)
      W=2.
   21 D1=CMPLX(0.,W)
      IF((C**2-4.*D).LT.0.0)  GO TO 26
      D2=CMPLX(C/2.-SQRT((C**2-4.*D)/4.),W)
      D3=CMPLX(C/2.+SQRT((C**2-4.*D)/4.),W)
      GO TO 28
   26 D2=CMPLX(C/2.,W-SQRT((4.*D-C**2)/4.))
      D3=CMPLX(C/2.,W+SQRT((4.*D-C**2)/4.))
   28 IF((A**2-4.*B).LT.0.0)GO TO 32
      D4=CMPLX(A/2.-SQRT((A**2-4.*B)/4.),W)
      D5=CMPLX(A/2.+SQRT((A**2-4.*B)/4.),W)
      GO TO 34
   32 D4=CMPLX(A/2.,W-SQRT((4.*B-A**2)/4.))
      D5=CMPLX(A/2.,W+SQRT((4.*B-A**2)/4.))
   34 D6=CMPLX(1.,T2*W)
      N1=CMPLX(1.,T1*W)
      IF(FIL.LT.1.0)GO TO 135
      N2=CMPLX(C/2.,W+SQRT((4.*D-C**2)/4.))
      N3=CMPLX(C/2.,W-SQRT((4.*D-C**2)/4.))
      D7=CMPLX(F/2.+SQRT((F**2-4.*D)/4.),W)
      D8=CMPLX(F/2.-SQRT((F**2-4.*D)/4.),W)
      GO TO 36
  135 G=K*(N1**2)/(((D1*D2*D3)+E)*D4*D5*(D6**2))
      GO TO 136
   36 G=K*(N1**2)*N2*N3/(((D1*D2*D3)+E)*D4*D5*(D6**2)*D/*D8)
  136 ABSVAL=CABS(G)
      GAIN=20.*ALOG10(ABSVAL)
      PHASE=(180./3.1415)*ATAN2(AIMAG(G),REAL(G))
      IF(PHASE.LE.0.)GO TO 38
      PHASE=-180.-(180.-PHASE)
   38 GC=G/(1.-G)
      AESC=CABS(GC)
```

```
      GAINC=20.*ALOG10(ABSC)
      PHASEC=(180./3.14159)*ATAN2(AIMAG(GC),REAL(GC))
      IF(PHASEC.LE.0.)GO TO 138
      PHASEC=-180.-(180.-PHASEC)
  138 WRITE(6,39)W,GAIN,PHASE,ABSC,GAINC,PHASEC
   39 FORMAT(6F12.4)
      IF(W.GE.10.)GO TO 43
      W=W+4.
      GO TO 21
   43 IF(W.GE.100.)GO TO 46
      W=W+10.
      GO TO 21
   46 IF(W.GE.2000.0)GO TO 48
      W=W+100.
      GO TO 21
   48 W=W+1000.
      IF(W.LE.4000.)GO TO 21
      CAP1=.00001
      RES1=T1/CAP1
      RES2=T2*RES1/(T1-T2)
      CAP3=.0000001
      CAP2=CAP3*(DRH**2)
      RES=1./(WH*SQRT(CAP2*CAP3))
      WRITE(6,75) CAP1,RES1,RES2,CAP2,CAP3,RES
   75 FORMAT(/6H CAP1=,2PE16.6,2X,5HRES1=,2PE16.6,2X,5HRES2=,2PE16.6,/
     1 6H CAP2=,2PE16.6,2X,5HCAP3=,2PE16.6,2X,5HRES =,2PE16.6)
      STOP
      END
```

```
$JOB,SI GORRAL-F-J*THESIS,F,,,17522013310
      CODE PLOT FOR OPEN AND CLOSED LOOP TRANSFER FUNCTION-FORCE
      REAL L,KA,KT,KV,KL,WH,WV,DRH,DRV,BE,A1,CT,C1,VT,I,KF,
     1 W,PHASE,GAIN,M,MU,A,B,C,D,E,ABSVAL,GAINC,ABSC,PHASEC,ML,
     2 T1,T2,FIL
      COMPLEX G,GC,D1,D2,D3,D4,D5,D6,N1,N2,N3,N4,N5,D7,D8
      READ(5,7)KA,KT,KV,AV,DRV,BE,A1,CT,C1,VT,K1,MT,T1,T2,FIL
    7 FORMAT( )
      WRITE(6,9) CT,K1,T1,T2
    9 FORMAT(4H CT=,F8.6,2X,3HK1=,F8.6,2X,3HT1=,F8.6,2X,3HT2=,F8.6,/)
      ML=.01695
      M=4.*BE*(A1**2)+4.*CT*C1*BE+VT*K1
      KL=(4.*BE*A1)/M
      KF=KL*ML
      WH=SQRT(M/(VT*MT))
      DRH=2.*CT*BE*SQRT(MT/(VT*M))+(C1/2.)*SQRT(VT/(MT*M))
      L=KA*KV*KT*KF*(AV**2)*(WH**2)
      A=2.*DRV*WV
      B=WV**2
      C=2.*DRH*WH
      D=WH**2
      E=(KL*(WH**2)*K)*CT)/(A1**2)
      DRP=(1.+2.*(DRH**2))/(2.*DRH)
      F=2.*DRP*WH
      WRITE(6,10)A,B,C,D,E,F
   10 FORMAT(4H A = ,F21.4,/4H B = ,F21.4,/4H C = ,F21.4,/
     1 4H D = ,F21.4,/4H E = ,F21.4,/4H F = ,F21.4)
      WRITE(6,19)KF,L,WH,DRH
   19 FORMAT(5H KF = ,F20.4,/4H L = ,F21.4,/5H WH = ,F20.4,/6H DRH =
     1 ,F19.4,//18X,9HOPEN LOOP,21X,11HCLOSED LOOP,13X//
     2 7H       W,9X,4HGAIN,8X,5HPHASE,6X,7HABSVALC,7X,
     3 9HGAINC,6X,6HPHASEC/10H    RAD/SEC,7X,2HDB,10X,3HDEG,
     4 22X,2HDB,10X,3HDEG)
      W=2.
   21 D1=CMPLX(.0,W)
      IF((C**2-4.*D).LT.0.0)  GO TO 26
      D2=CMPLX(C/2.-SQRT((C**2-4.*D)/4.),W)
      D3=CMPLX(C/2.+SQRT((C**2-4.*D)/4.),W)
      GO TO 28
   26 D2=CMPLX(C/2.,W-SQRT((4.*D-C**2)/4.))
      D3=CMPLX(C/2.,W+SQRT((4.*D-C**2)/4.))
   28 IF((A**2-4.*B).LT.0.0)GO TO 32
      D4=CMPLX(A/2.-SQRT((A**2-4.*B)/4.),W)
      D5=CMPLX(A/2.+SQRT((A**2-4.*B)/4.),W)
      GO TO 34
   32 D4=CMPLX(A/2.,W-SQRT((4.*B-A**2)/4.))
      D5=CMPLX(A/2.,W+SQRT((4.*B-A**2)/4.))
   34 D6=CMPLX(1.,T2*W)
      N1=CMPLX(1.,T1*W)
      N4=CMPLX(5.6217,W)
      N5=CMPLX(19.5166,W)
      IF(FIL.LT.1.0)GO TO 135
      N2=CMPLX(C/2.,W+SQRT((4.*D-C**2)/4.))
      N3=CMPLX(C/2.,W-SQRT((4.*D-C**2)/4.))
      D7=CMPLX(F/2.+SQRT((F**2-4.*D)/4.),W)
      D8=CMPLX(F/2.-SQRT((F**2-4.*D)/4.),W)
      GO TO 36
  135 G=L*(N1**2)*N4*N5/(((D1*D2*D3)+D1*D4*D5*(D6**2))
      GO TO 136
   36 G=L*(N1**2)*N2*N3*N4*N5/(((D1*D2*D3)+D1*D4*D5*(D6**2)*D7*D8)
  136 ABSVAL=CABS(G)
      GAIN=20.*ALOG10(ABSVAL)
      PHASE=(180./3.14159)*ATAN2(AIMAG(G),REAL(G))
```

```
      GC=G/(1.+G)
      ABSC=CABS(GC)
      GAINC=20.*ALOG10(ABSC)
      PHASEC=(180./3.14159)*ATAN2(AIMAG(GC),REAL(GC))
  136 WRITE(6,39)W,GAIN,PHASE,ABSC,GAINC,PHASEC,G,GC
   39 FORMAT(6F12.4,4E12.4)
      IF(W.GE.10.)GO TO 43
      W=W+4.
      GO TO 21
   43 IF(W.GE.100.)GO TO 46
      W=W+10.
      GO TO 21
   46 IF(W.GE.2000.0)GO TO 48
      W=W+100.
      GO TO 21
   48 W=W+1000.
      IF(W.GE.20000.)GO TO 21
      CAP1=.00001
      RES1=T1/CAP1
      RES2=T2*RES1/(T1-T2)
      CAP3=.000001
      CAP2=CAP3*(DRM**2)
      RES=1./(WM*SQRT(CAP2*CAP3))
      WRITE(6,75) CAP1,RES1,RES2,CAP2,CAP3,RES
   75 FORMAT(/6H CAP1=,2PE16.6,2X,5HRES1=,2PE16.6,2X,5HRES2=,2PE16.6,/
     1 6H CAP2=,2PE16.6,2X,5HCAP3=,2PE16.6,2X,5HRES =,2PE16.6)
      STOP
      END
```

```
LET,SI CORRAL-F-J*TRL,ONE,,,211226073110
      TRANSIENT RESPONSE
      DIMENSION P(10),L(10),R(9),FT(10),RT(300),RT1(300),FT1(10),L1(11)
     1 ,RES(300),RES1(300)
      REAL KR,KA,KT,KV,KL,WH,WV,DRH,DRV,DE,A1,CT,C1,VT,K1,
     1 M,MT,A,B,C,D,E,T1,T2
      INTEGER Y
      COMPLEX P,R,N1,N3,N4,RT,FT,L,RT1,FT1,L1
      READ(5,7)KA,KT,KV,WV,DRV,DE,A1,CT,C1,VT,K1,MT,T1,T2
    7 FORMAT()
      READ(5,11)N,EPS,KMAX
   11 FORMAT()
      WRITE(6,5)CT,K1,T1,T2
    5 FORMAT(4H CT=,F8.6,2X,3HK1=,F8.6,2X,3HT1=,F8.6,2X,3HT2=,F8.6,/)
      M=4.*DE*(A1**2)+4.*CT*C1*DE+VT*K1
      KL=(4.*DE*A1)/M
      WH=SQRT(M/(VT*MT))
      DRH=2.*CT*DE*SQRT(MT/(VT*M))+(C1/2.)*SQRT(VT/(MT*M))
      KR=KA*KV*KT*KL
      A=2.*DRV*WV
      B=WV**2
      E=2.*DRH*WH
      D=WH**2
      C=(KL*(WH**2)*K1*CT)/(A1**2)
      DRP=(1.+2.*(DRH**2))/(2.*DRH)
      F=2.*DRP*WH
      WRITE(6,10)A,B,C,D,E,F
   10 FORMAT(4H A = ,F21.4,/4H B = ,F21.4,/4H C = ,F21.4,/
     1 4H D = ,F21.4,/4H E = ,F21.4,/4H F = ,F21.4)
      WRITE(6,19)KL,KR,WH,DRH,DRP
   19 FORMAT(3H KL = ,F20.4,/3H KR = ,F20.4,/3H WH = ,F20.4,/6H DRH =
     1 ,F19.4,/6H DRP = ,F19.4)
      D1=(C+A)/(B*D)
      D2=(D+A*C+B)/(B*D)
      D3=(E+A*D+B*C)/(B*D)
      D4=(A*E+B*D)/(B*D)
      D5=(B*E)/(B*D)
      D6=(T2**2)*F+2.*T2
      D7=(T2**2)*D+1.+2.*T2*F
      D8=F+2.*T2*D
      D9=KR*(T1**2)
      D10=KR*((T1**2)*C+2.*T1)
      D11=KR*((T1**2)*D+1.+2.*T1*C)
      D12=KR*(C+2.*T1*D)
      D13=KR*D
      P(1)=CMPLX(D5*D+D13,.0)
      P(2)=CMPLX(D4*D+D5*D8+D12,.0)
      P(3)=CMPLX(D3*D+D4*D8+D5*D7+D11,.0)
      P(4)=CMPLX(D2*D+D3*D8+D4*D7+D5*D6+D10,.0)
      P(5)=CMPLX(D1*D+D2*D8+D3*D7+D4*D6+D5*(T2**2)+D9,.0)
      P(6)=CMPLX(D/(B*D)+D1*D8+D2*D7+D3*D6+D4*(T2**2),.0)
      P(7)=CMPLX(D8/(B*D)+D1*D7+D2*D6+D3*(T2**2),.0)
      P(8)=CMPLX(D7/(B*D)+D1*D6+D2*(T2**2),.0)
      P(9)=CMPLX(D6/(B*D)+D1*(T2**2),.0)
      P(10)=CMPLX((T2**2)/(B*D),.0)
      P1=REAL(P(1))
      P2=REAL(P(2))
      P10=REAL(P(10))
      PRINT 55
   55 FORMAT(//14X,4HREAL,18X,9HIMAGINARY,/)
      WRITE(6,57) (I,P(I),I=1,10)
   57 FORMAT(3H P(,I2,2H)=,2P2E22.6)
      PRINT 59
```

```
 59   FORMAT(/27X,5HROOTS,/)
      CALL ROOTCP(P,N,EPS,KMAX,R,J,$62)
      GO TO 65
 62   WRITE(6,63) J
 63   FORMAT(//34H ERROR RETURN NUMBER OF ITERATIONS,
     1 13H EXCEEDED FOR,I2,8H TH ROOT)
 65   WRITE(6,66) (I,R(I),I=1,J)
 66   FORMAT(3H R(,I2,2H)=,2P2E22.8)
      IF(J.LT.9) GO TO 106
      N1=CMPLX(-1./T1,0.)
      N3=CMPLX(-C/2.,SQRT((4.*D-C**2)/4.))
      N4=CONJG(N3)
      L(1)=(KR*(T1**2)*(-N1)**2)*(-N3)*(-N4))/(
     1 P10*(-R(1))*(-R(2))*(-R(3))*(-R(4))*
     2 (-R(5))*(-R(6))*(-R(7))*(-R(8))*(-R(9)))
      L(2)=(KR*(T1**2)*((R(1)-N1)**2)*(R(1)-N3)*(R(1)-N4))/(R(1)*
     1 P10*(R(1)-R(2))*(R(1)-R(3))*(R(1)-R(4))*
     2 (R(1)-R(5))*(R(1)-R(6))*(R(1)-R(7))*(R(1)-R(8))*(R(1)-R(9)))
      L(3)=(KR*(T1**2)*((R(2)-N1)**2)*(R(2)-N3)*(R(2)-N4))/(R(2)*
     1 P10*(R(2)-R(1))*(R(2)-R(3))*(R(2)-R(4))*
     2 (R(2)-R(5))*(R(2)-R(6))*(R(2)-R(7))*(R(2)-R(8))*(R(2)-R(9)))
      L(4)=(KR*(T1**2)*((R(3)-N1)**2)*(R(3)-N3)*(R(3)-N4))/(R(3)*
     1 P10*(R(3)-R(1))*(R(3)-R(2))*(R(3)-R(4))*
     2 (R(3)-R(5))*(R(3)-R(6))*(R(3)-R(7))*(R(3)-R(8))*(R(3)-R(9)))
      L(5)=(KR*(T1**2)*((R(4)-N1)**2)*(R(4)-N3)*(R(4)-N4))/(R(4)*
     1 P10*(R(4)-R(1))*(R(4)-R(2))*(R(4)-R(3))*
     2 (R(4)-R(5))*(R(4)-R(6))*(R(4)-R(7))*(R(4)-R(8))*(R(4)-R(9)))
      L(6)=(KR*(T1**2)*((R(5)-N1)**2)*(R(5)-N3)*(R(5)-N4))/(R(5)*
     1 P10*(R(5)-R(1))*(R(5)-R(2))*(R(5)-R(3))*(R(5)-R(4))*
     2 (R(5)-R(6))*(R(5)-R(7))*(R(5)-R(8))*(R(5)-R(9)))
      L(7)=(KR*(T1**2)*((R(6)-N1)**2)*(R(6)-N3)*(R(6)-N4))/(R(6)*
     1 P10*(R(6)-R(1))*(R(6)-R(2))*(R(6)-R(3))*(R(6)-R(4))*
     2 (R(6)-R(5))*(R(6)-R(7))*(R(6)-R(8))*(R(6)-R(9)))
      L(8)=(KR*(T1**2)*((R(7)-N1)**2)*(R(7)-N3)*(R(7)-N4))/(R(7)*
     1 P10*(R(7)-R(1))*(R(7)-R(2))*(R(7)-R(3))*(R(7)-R(4))*
     2 (R(7)-R(5))*(R(7)-R(6))*(R(7)-R(8))*(R(7)-R(9)))
      L(9)=(KR*(T1**2)*((R(8)-N1)**2)*(R(8)-N3)*(R(8)-N4))/(R(8)*
     1 P10*(R(8)-R(1))*(R(8)-R(2))*(R(8)-R(3))*(R(8)-R(4))*
     2 (R(8)-R(5))*(R(8)-R(6))*(R(8)-R(7))*(R(8)-R(9)))
      L(10)=(KR*(T1**2)*((R(9)-N1)**2)*(R(9)-N3)*(R(9)-N4))/(R(9)*
     1 P10*(R(9)-R(1))*(R(9)-R(2))*(R(9)-R(3))*(R(9)-R(4))*
     2 (R(9)-R(5))*(R(9)-R(6))*(R(9)-R(7))*(R(9)-R(8)))
      DO 204 I=2,10
      J=I-1
204   L1(I)=L(I)/R(J)
      L1(1)=L(1)
      PRINT 103
103   FORMAT(/36X,9HCONSTANTS,/23X,4HSTEP,26X,4HRAMP,/)
      WRITE(6,104) (I,L(I),L1(I),I=1,10)
104   FORMAT(3H L(,I2,2H)=,2P4E16.6)
      PRINT 108
108   FORMAT(7H1T(SEC),4X,8HF(T)STEP,6X,8HF(T)RAMP)
      FT(1)=REAL(L(1))
      FT10=(KR*2.*T1*D*P1+KR*C*P1-KR*D*P2)/(P1**2)
      T=0.
      DO 128 Y=1,56
      FT1(1)=FT(1)*T
      DO 124 I=2,9
      J=I-1
      FT(I)=L(I)*CEXP(R(J)*T)
124   FT1(I)=(L1(I))*CEXP(R(J)*T)
      FT(10)=REAL(L(10))*CEXP(REAL(R(9))*T)
      FT1(10)=(REAL(L1(10)))*(CEXP(REAL(R(9))*T))
```

```
      RT(Y)=FT(1)+FT(2)+FT(3)+FT(4)+FT(5)+FT(6)+FT(7)+FT(8)+
     1 FT(9)+FT(10)
      RT1(Y)=FT1(0+FT1(1)+FT1(2)+FT1(3)+FT1(4)+FT1(5)+FT1(6)+FT1(7)+
     1 FT1(8)+FT1(9)+FT1(10)
      RES(Y)=REAL(RT(Y))
      RES1(Y)=REAL(RT1(Y))
      WRITE(6,131) T,RES(Y),RES1(Y)
      IF(T.GT..019) GO TO 126
      T1=T+.001
      GO TO 128
  126 IF(T.GT..14) GO TO 228
      T1=T+.01
      GO TO 128
  228 IF(T.GT..95) GO TO 338
      T1=T+.05
      GO TO 128
  338 T1=T+.2
  128 T=T1
  131 FORMAT(F7.4,2F12.5)
      WRITE(6,240) FT1(
  240 FORMAT(/7H ERROR=,2P2E16.6)
  106 STOP
      END
```

```
&LET,SI CORRAL-F-J*FORCE.ONE,,,125600140410
      TRANSIENT RESPONSE-FORCE
      DIMENSION P(10),L(10),R(9),FT(10),RT(300),RT1(300),FT1(10),L1(11)
     1 ,RES(300),RES1(300)
      REAL KR,KA,KT,KV,KL,WH,WV,DRH,DRV,DE,A1,CT,C1,VT,K1,
     1 M,MT,A,B,C,D,E,KF,ML
      INTEGER Y
      COMPLEX P,R,N1,N2,N3,N4,RT,FT,L,RT1,FT1,L1
      READ(5,7)KA,KT,KV,WV,DRV,DE,A1,CT,C1,VT,K1,MT
    7 FORMAT()
      READ(5,11)N,EPS,KMAX
   11 FORMAT()
      WRITE(6,5)CT,DE
    5 FORMAT(4H CT=,F8.6,2X,3HDE=,F12.8)
      M=4.*DE*(A1**2)+4.*CT*C1*DE+VT*K1
      KL=(4.*DE*A1)/M
      ML=.01695
      KF=KL*ML
      WH=SQRT(M/(VT*MT))
      DRH=2.*CT*DE*SQRT(MT/(VT*M))+(C1/2.)*SQRT(VT/(MT*M))
      KR=KA*KT*KV*KF
      A=2.*DRV*WV
      B=WV**2
      C=2.*DRH*WH
      D=WH**2
      E=(KL*(WH**2)+K1*CT)/(A1**2)
      DRP=(1.+2.*(DRH**2))/(2.*DRH)
      F=2.*DRP*WH
      WRITE(6,10)A,B,C,D,E,F
   10 FORMAT(4H A = ,F21.4,/4H B = ,F21.4,/4H C = ,F21.4,/
     1 4H D = ,F21.4,/4H E = ,F21.4,/4H F = ,F21.4)
      WRITE(6,19)KF,KR,WH,DRH,DRP
   19 FORMAT(5H KF = ,F20.4,/5H KR = ,F20.4,/5H WH = ,F20.4,/6H DRH =
     1 ,F19.4,/6H DRP = ,F19.4)
      D1=(C+A)/(B*D)
      D2=(D+A*C+B)/(B*D)
      D3=(E+A*D+B*C)/(B*D)
      D4=(A*E+B*D)/(B*D)
      D5=E/B
      D6=KR*(25.14+C)
      D7=KR*(109.725625+C*25.14+D)
      D8=KR*(C*109.725625+D*25.14)
      D9=KR*D*109.725625
      P(1)=CMPLX(D5*D+D9,.0)
      P(2)=CMPLX(D4*D+D5*F+D8,.0)
      P(3)=CMPLX(D3*D+D4*F+D5+D7,.0)
      P(4)=CMPLX(D2*D+D3*F+D4+D6,.0)
      P(5)=CMPLX(D1*D+D2*F+D3+KR,.0)
      P(6)=CMPLX(1./B+D1*F+D2,.0)
      P(7)=CMPLX(F/(B*D)+D1,.0)
      P(8)=CMPLX(1./(B*D),.0)
      P1=REAL(P(1))
      P2=REAL(P(2))
      P8=REAL(P(8))
      PRINT 55
   55 FORMAT(//14X,4HREAL,16X,9HIMAGINARY,/)
      WRITE(6,57) (I,P(I),I=1,8)
   57 FORMAT(3H P(,I2,2H)=,2P2L22.8)
      PRINT 59
   59 FORMAT(/27X,5HROOTS,/)
      CALL ROOTCP(P,N,EPS,KMAX,R,J,*62)
      GO TO 65
   62 WRITE(6,63) J
```

```
63  FORMAT(//34H ERROR RETURN NUMBER OF ITERATIONS,
     1 13H EXCEDEED FOR,I2,8H TH ROOT)
 65  WRITE(6,66) (I,R(I),I=1,J)
 66  FORMAT(3H R(,I2,2H)=,2P2E22.8)
     IF(J.LT.7) GO TO 106
     N1=CMPLX(-C/2.,SQRT((4.*D-C**2)/4.))
     N2=CONJG(N1)
     N3=CMPLX(-5.621,.0)
     N4=CMPLX(-15.5183,.0)
     L(1)=(KR*(-N1)*(-N2)*(-N3)*(-N4))/(P8*
    1 (-R(1))*(-R(2))*(-R(3))*(-R(4))*(-R(5))*
    2 (-R(6))*(-R(7)))
     L(2)=(KR*(R(1)-N1)*(R(1)-N2)*(R(1)-N3)*(R(1)-N4))/(P8*R(1)*
    1 (R(1)-R(2))*(R(1)-R(3))*(R(1)-R(4))*(R(1)-R(5))*
    2 (R(1)-R(6))*(R(1)-R(7)))
     L(3)=(KR*(R(2)-N1)*(R(2)-N2)*(R(2)-N3)*(R(2)-N4))/(P8*R(2)*
    1 (R(2)-R(1))*(R(2)-R(3))*(R(2)-R(4))*(R(2)-R(5))*
    2  (R(2)-R(6))*(R(2)-R(7)))
     L(4)=(KR*(R(3)-N1)*(R(3)-N2)*(R(3)-N3)*(R(3)-N4))/(P8*R(3)*
    1 (R(3)-R(1))*(R(3)-R(2))*(R(3)-R(4))*(R(3)-R(5))*
    2 (R(3)-R(6))*(R(3)-R(7)))
     L(5)=(KR*(R(4)-N1)*(R(4)-N2)*(R(4)-N3)*(R(4)-N4))/(P8*R(4)*
    1 (R(4)-R(1))*(R(4)-R(2))*(R(4)-R(3))*(R(4)-R(5))*
    2 (R(4)-R(6))*(R(4)-R(7)))
     L(6)=(KR*(R(5)-N1)*(R(5)-N2)*(R(5)-N3)*(R(5)-N4))/(P8*R(5)*
    1 (R(5)-R(1))*(R(5)-R(2))*(R(5)-R(3))*(R(5)-R(4))*
    2 (R(5)-R(6))*(R(5)-R(7)))
     L(7)=(KR*(R(6)-N1)*(R(6)-N2)*(R(6)-N3)*(R(6)-N4))/(P8*R(6)*
    1 (R(6)-R(1))*(R(6)-R(2))*(R(6)-R(3))*(R(6)-R(4))*(R(6)-R(5))*
    2 (R(6)-R(7)))
     L(8)=(KR*(R(7)-N1)*(R(7)-N2)*(R(7)-N3)*(R(7)-N4))/(P8*R(7)*
    1 (R(7)-R(1))*(R(7)-R(2))*(R(7)-R(3))*(R(7)-R(4))*(R(7)-R(5))*
    2 (R(7)-R(6)))
     DO 204 I=2,8
     J=I-1
204  L1(I)=L(I)/R(J)
     L1(1)=L(1)
     PRINT 103
103  FORMAT(/30X,9HCONSTANTS,/29X,4HSTEP,28X,4HRAMP,/)
     WRITE(6,104) (I,L(I),L1(I),I=1,8)
104  FORMAT(3H L(,I2,2H)=,2P4E16.6)
     PRINT 108
108  FORMAT(7HIT(SEC),4X,8HF(T)STEP,6X,8HF(T)RAMP)
     FT(1)=REAL(L(1))
     FT1(1)=REAL((L*(109.725625+25.14*D)*P1-(P2*D*109.725625))/(P1**2)
     T=0.
     DO 123 Y=1,56
     FT1(1)=FT(1)*T
     DO 124 I=2,8
     J=I-1
     FT(I)=L(I)*CEXP(R(J)*T)
124  FT1(I)=(L1(I))*CEXP(R(J)*T)
     RT(Y)=FT(1)+FT(2)+FT(3)+FT(4)+FT(5)+FT(6)+FT(7)+FT(8)
     RT1(Y)=FT1(1)+FT1(1)+FT1(2)+FT1(3)+FT1(4)+FT1(5)+FT1(6)+FT1(7)+
    1 FT(8)
     RES(Y)=REAL(RT(Y))
     RES1(Y)=REAL(RT1(Y))
     WRITE(6,131) T,RES(Y),RES1(Y)
     IF(T.GT..019) GO TO 126
     T=T+.001
     GO TO 128
126  IF(T.GT..14) GO TO 228
     T=T+.01
```

```
      GO TO 128
200   IF(T.GT..95) GO TO 338
      T1=T+.05
      GO TO 128
300   T1=T+.2
100   T=T1
101   FORMAT(F7.4,2F14.9)
      WRITE(6,240)ET10
240   FORMAT(/7H ERROR=,2P2E16.6)
106   STOP
      END
```

APPENDIX IV

EVALUATING THE COMPONENTS OF THE COMPENSATORS

Bridged-T Network

Rewriting equations (24) and (25):

$$C_2 = C_3 \xi_h^2$$

$$R = \frac{1}{\omega_h [C_2 C_3]^{1/2}}$$

Setting C_3 to an arbitrary value of

$$C_3 = .07 \ \mu f$$

and considering the extreme cases for ω_h and ξ_h

$$\omega_h = 1{,}255.1091 \text{ rad/sec} \rightarrow \xi_h = .0291$$

$$\omega_h = 2{,}335.603 \text{ rad/sec} \rightarrow \xi_h = .0038$$

$$C_{2\ min} = (.7)(.0038)^2 \times 10^{-7} = .999 \text{ pf}$$

$$C_{2\ max} = (.7)(.0291)^2 \times 10^{-7} = 59.3 \text{ pf}$$

$$R_{min} = \frac{10^9}{(1255.1091)[(5.93)(.7)]}^{1/2} = 391.2 \text{ K}\Omega$$

$$R_{max} = \frac{10^9}{(2,335.603)[(.999)(.07)]^{1/2}} = 1,619.0\ K\Omega$$

Therefore, the values to be used are

C_3 = .07 μf (fixed capacitor)

C_2 = 1.0 to 60.0 pf (variable capacitor)

R = 0.0 to 1.7 MΩ (variable resistor)

Lead Network

The equations that hold in this case are

$$R_1 = \frac{T_1}{C_1}$$

$$R_2 = \frac{T_2 R_1}{T_1 - T_2}$$

Setting C_1 to a fixed value of

$$C_1 = 10\ \mu f$$

The ranges of interest for T_1 and T_2 are:

T_1 = .033 to .1 sec

T_2 = .0033 to .01 sec

Therefore,

$$R_{1max} = \frac{.1}{10^{-5}} = 10\ K\Omega$$

$$R_{1min} = \frac{.033}{10^{-5}} = 3.333\ K\Omega$$

$$R_{2min} = \frac{(.0033)(3.333)(10^{3})}{.033-.0033} = 370\ \Omega$$

$$R_{2max} = \frac{(.01)(3.333)(10^{3})}{.033-.01} = 1.43\ K\Omega$$

Thus, the values to be used are

C_1 = 10μf (fixed capacitor)

R_1 = .0 to 10.0 KΩ (variable resistor)

R_2 = 0.0 to 1.5 KΩ (variable resistor)

BIBLIOGRAPHY

Literature Cited

1. J. F. Fulton and J. Pi-Suñer, "A Note Concerning the Probable Function of Various Afferent End-Organs in Skeletal Muscle," Amer. J. Physiology, Vol. 83, 1928, pp. 554-562.

2. B. H. C. Matthews, "Nerve Endings in Mammalian Muscle," J. Physiology, Vol. 78, 1933, pp. 1-53.

3. R. E. Poppele and C. A. Terzuolo, "Myotatic Reflex: Its Input-Output Relation," Science, Vol. 159, 1968, pp. 743-745.

4. R. E. Poppele and R. J. Bowman, "Quantitative Description of Linear Behavior of Mammalian Muscle Spindles," J. Neurophysiology, Vol. 33, 1970, pp. 59-72.

5. N. P. Rosenthal, T. A. McKean, W. J. Roberts and C. A. Terzuolo, "Frequency Analysis of Stretch Reflex and Its Main Subsystems in Triceps Surae Muscles of the Cat," J. Neurophysiology, Vol. 33, 1970, pp. 713-749.

6. W. J. Roberts, N. P. Rosenthal and C. A. Terzuolo, "A Control Model of Stretch Reflex," J. Neurophysiology, Vol. 34, 1971, pp. 620-634.

7. D. R. Wilkie, "Measurement of the Series Elastic Component at Various Times During a Single Muscle Twitch," J. Physiology, Vol. 134, 1959, pp. 327-530.

8. M. M. Civan and R. J. Podolsky, "Contraction Kinetics of Striated Muscle Following Quick Changes in Load," J. Physiology, Vol. 184, 1966, pp. 511-534.

9. H. L. McCrovey, H. H. Gale and N. R. Alpert, "Mechanical Properties of Cat Tenuissimus Muscle," Amer. J. Physiology, Vol. 210, 1966, pp. 114-120.

10. G. Lennerstrand, and U. Thoden, "Dynamic Analysis of Muscle Spindle Endings in the Cat Using Length Changes of Different Length-Time Relations, Acta Physiol. Scand., Vol. 63, 1968, pp. 234-250.

11. D Stuart, K. Ott, K. Ishikava, and E. Eldred, "Muscle Receptor Responses to Sinusoidal Stretch," Exp.Neurol., Vol. 13, 1965,p.82-95.

12. P. B. C. Matthews, and R. B. Stein, "The Sensitivity of Muscle Spindle Afferents to Small Sinusoidal Changes of Length," J. Physiology, Vol. 200, 1969, pp. 723-743.

13. E. Alnaes, J. K. S. Jansen, and T. Rudjord, "Fusimotor Activity in the Spinal Cat," Acta Physiol. Scand., Vol. 63, 1965, pp. 197-212.

14. P. B. C. Matthews, "The Dependence of Tension Upon Extension in the Stretch Reflex of the Soleus Muscle of the Decerebrate Cat," J. Physiology, Vol. 147, 1959, pp. 521-546.

15. N. F. Clinch, and V. A. Tennant, "A Loudspeaker Servo System for Use in Studying Muscle Mechanics," J. Appl. Physiology, Vol. 32, 1972, pp. 703-705.

16. K. E. Machin, and J. W. S. Pringle, "The Physiology of Insect Fibrillar Muscle. II Mechanical Properties of a Beetle Flight Muscle," Proc. Roy. Soc., Series B, 151, 1959, pp. 204-225.

17. M. C. Brown, I. Engberger, and P. B. C. Matthews,"The Relative Sensitivity to Vibration of Muscle Receptors of the Cat," J. Physiology, Vol. 192, 1967, pp. 773-800.

18. P. B. C. Matthews, "The Differentiation of Two Types of Fusimotor Fiber by Their Effects on the Dynamic Response of Muscle Spindle Primary Endings," Quart. J. Exptl. Physiology, Vol. 47, 1962, pp. 324-333.

19. W. J. Thayer, "Transfer Functions for Moog Servovalves," Technical Bulletin No. 103, Moog Servocontrols, Inc., 1965, p. 11.

20. P. N. Nikiforuk and D. R. Westlund, "The Large Signal Response of a Loaded High-Pressure Hydraulic Servomechanism," Proc. Inst. Mech. Eng., Vol. 180, pt. 1, 1966, pp. 557-577.

21. G. B. Keller, Hydraulic System Analysis, Industrial Publishing Co., 1970, pp. 114-117.

22. H. E. Merrit, Hydraulic Control Systems, John Wiley and Sons, Inc., 1967, pp. 132-152, 224-234.

23. A. Crowe, "A Mechanical Model of Muscle and its Application to the Intrafusal Fibers of the Mammalian Muscle Spindle," J. Biomechanics, Vol. 3, 1970, pp. 583-592.

24. J. W. Pringle, "Models of Muscles," from Models and Analogues in Biology, Symp. Soc. Exptl. Biology, No. 14, 1960, pp. 41-68.

25. P. Chandaket and A. B. Rosenstein, "Notes on Bridged-T Complex Conjugate Compensation and Four Terminal Network Loading," AIEE Transactions, Applications and Insustry, July 1959, pp. 148-163.

26. H. L. Harrison and J. G. Bollinger, Introduction to Automatic Controls, International Textbook Co., July 1970, pp. 176-178.

27. B. C. Kuo, Automatic Control Systems, Prentice Hall, Inc., 1967, pp. 225-226.

Other References

Blackburn, J. F., Reethof, G. and Shearer, J. L., Fluid Power Control, The Technology Press of M.I.T. and John Wiley and Sons, Inc., 1960, 710 p .

Crowe, A., "A Mechanical Model of the Mammalian Muscle Spindle," J. Theoretical Biology, Vol. 21, 1968, pp. 21-41.

Dransfield, P., Engineering Systems and Automatic Control, Prentice Hall, Inc., 1968, 429 p .

Gillon, M., Hydraulic Servo Systems, Analysis and Design, Plenum Press, 1969, 462 p .

"Moog Type Thirty Servovalves," Moog General Information, Moog Servocontrols, Inc.

Nixon, F. E., Handbook of Laplace Transformation, Prentice-Hall, Inc. 1965, 260 p.